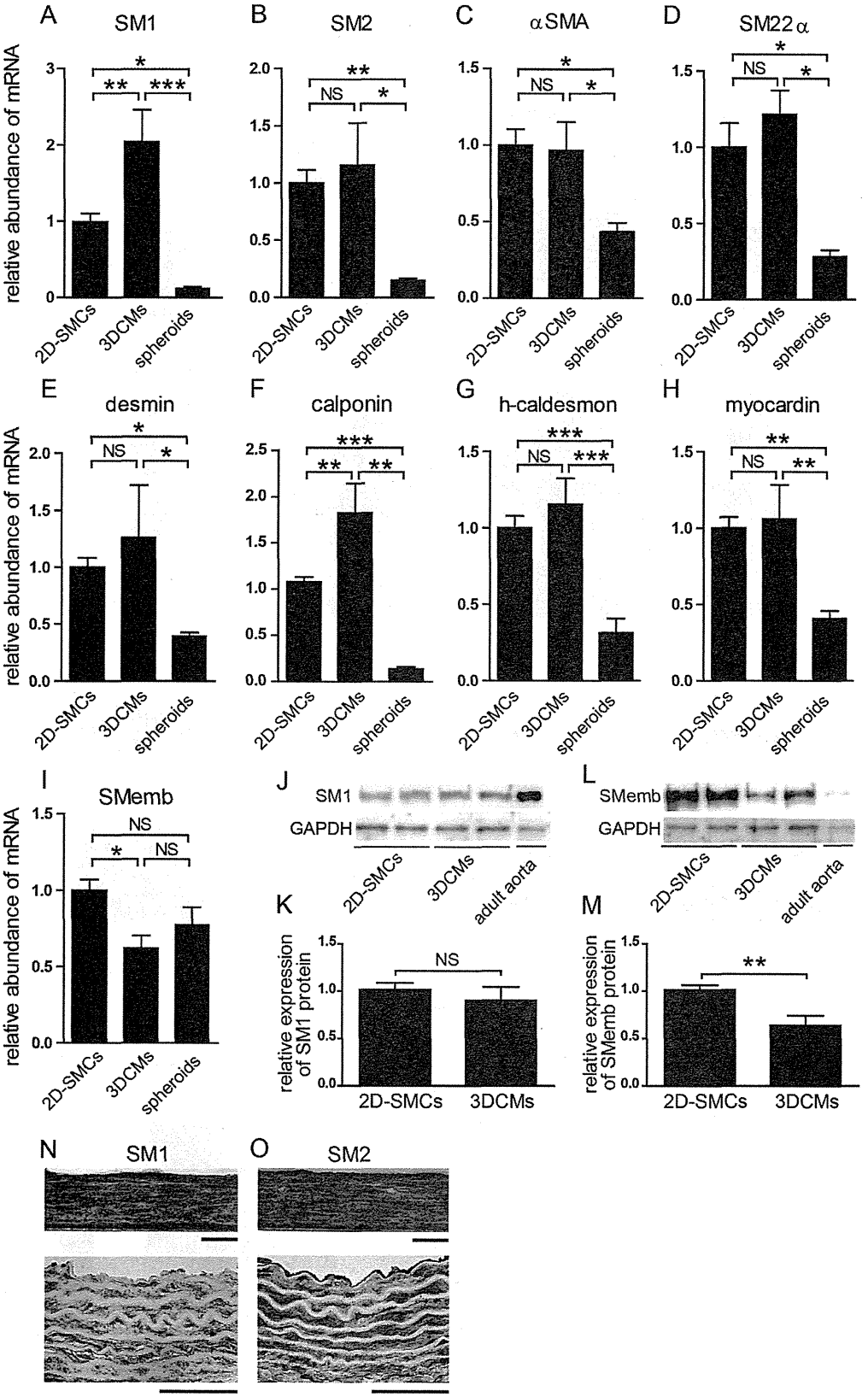

Fig. 3. Characterization of SMC phenotype in 3DCMs. (A–H) Messenger RNA expressions of differentiation SMC markers, SM1 (A), SM2 (B), αSMA (C), SM22α (D), desmin (E), calponin (F), h-caldesmon (G), myocardin (H), and a dedifferentiation SMC marker, SMemb (I) in 2D-SMCs, 3DCMs, and SMC spheroids. $n = 4–8$. (J) Immunoblot analysis for SM1 in 2D-SMCs and 3DCMs. Rat adult aorta was used as positive control. (K) Quantification of (J). $n = 10$. (L) Immunoblot analysis for SMemb in 2D-SMCs and 3DCMs. (M) Quantification of (L). $n = 10$. *, $p < 0.05$; **, $p < 0.01$; ***, $p < 0.001$. NS: not significant. Immunohistochemistry for SM1 (N) and SM2 (O). Brown color indicates positive staining. top panels: 3DCMs. Scale bars: 10 μm lower panels: rat adult aorta. Scale bars: 50 μm.

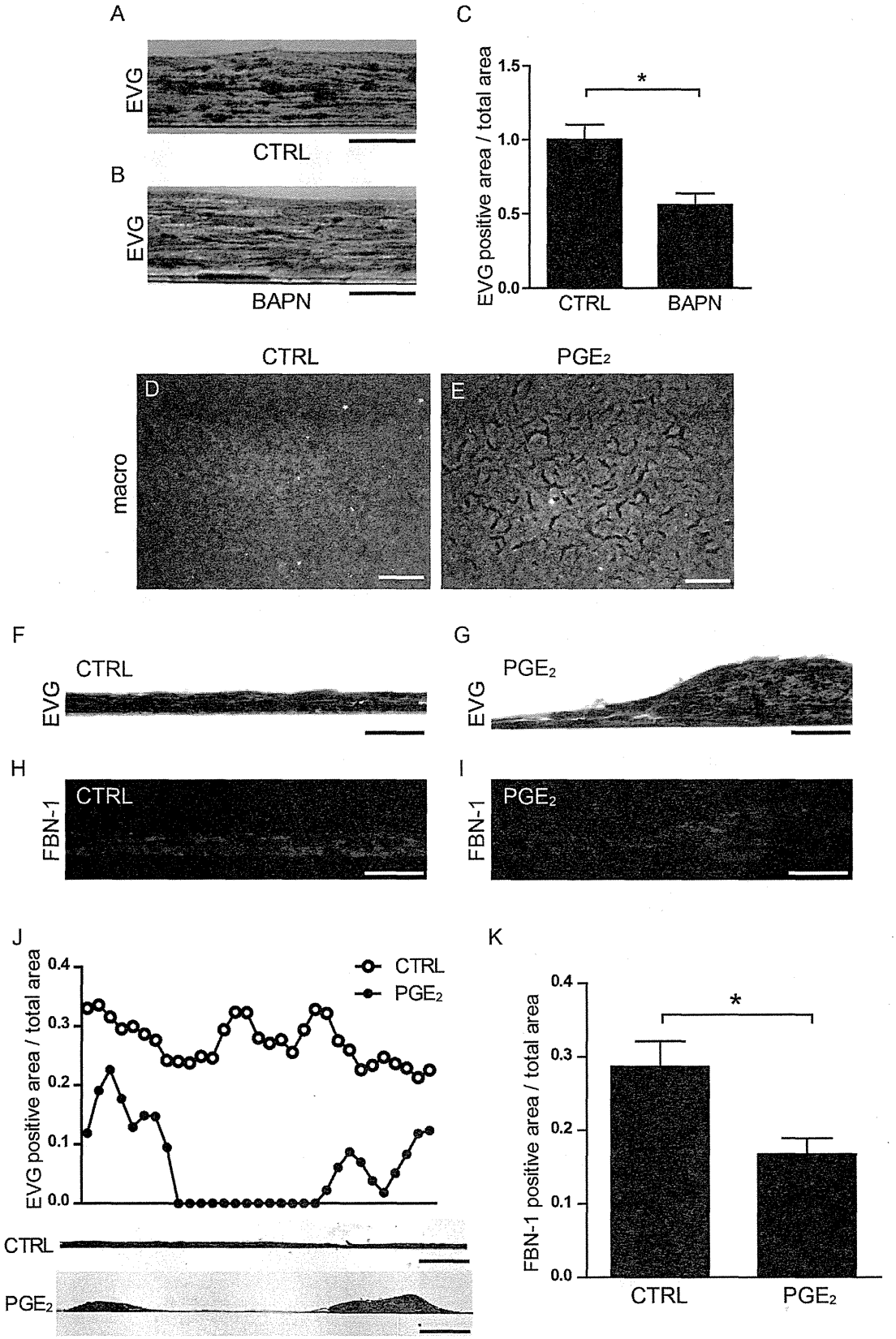

Fig. 4. Pharmacological manipulation of elastic fiber formation in 3DCMs. (A–B) EVG stain of 3DCMs. CTRL (A), and BAPN (1 μM) stimulation (B). Scale bars: 10 μm. (C) Quantification of the density of elastic fibers in (A) and (B). $n = 5$. (D–E) Macroscopic images of 3DCMs treated with or without PGE_2 (1 μM) (PGE_2 and CTRL, respectively). Scale bars:

SMC differentiation in this culture system in comparison to 2D-SMCs and SMC spheroids by monitoring the expression of various SMC markers.

It has been reported that the expression levels of differentiation SMC markers, such as SM1, SM2, αSMA, SM22α, and desmin, were highly expressed in the medial layer of SMCs but reduced in human subendotherial intima of atherosclerotic lesions [30–33] and human and rabbit aortic aneurysmal lesions [34,35]. Differentiation SMC markers such as the high molecular weight isoform of caldesmon (h-caldesmon) and calcium-binding protein calponin are also suggested to be downregulated in human atheromatous intima [31,32]. The serum response factor coactivator gene myocardin is required for the expression of many SMC differentiation marker genes and for the initial differentiation of SMC [29]. SMemb is known to be a dedifferentiation SMC marker that is abundantly expressed in human fetal arteries and immature adult cells that are present in vascular injury-induced intima [29]. Expression analysis of mRNAs demonstrated that most differentiation markers were similarly expressed between 2D-SMCs and 3DCMs (Fig. 3A–H). Although the expression levels of SM1 mRNA were higher in 3DCMs than in 2D-SMCs, the SM1 protein expression did not differ between these two culture systems (Fig. 3J–K). Among the SMC phenotypic markers examined, only SMemb was reduced in the 3DCMs compared to the 2D-SMCs in both mRNA and protein (Fig. 3I, L,M).

We also examined the SMC phenotypes of SMC spheroids in comparison with 3DCMs. mRNA expressions of all differentiation SMC markers examined in the whole spheroids were lower than in 3DCMs and even 2D-SMCs (Fig. 3A–H). The expression level of SMemb mRNA in the spheroids was similar to 2D-SMCs and 3DCMs.

Immunohistochemistry showed that SM1 and SM2 proteins were homogenously expressed in 3DCMs (Fig. 3N,O). In SMC spheroids, SM1 and SM2 were expressed mainly in the outer shell, while the dedifferentiation marker SMemb was expressed in the porous core (Supplemental Fig. 5D,F).

These data suggested that the 3DCMs exhibited similar SMC phenotypes to 2D-SMCs, although a differentiated phenotype was maintained compared to the other types of 3D culture, i.e., SMC spheroids.

3.4. Pharmacological manipulation of elastic fiber formation in 3DCMs

To examine the molecular mechanisms of the elastogenesis and degradation of elastic fibers, and to explore new therapeutic strategies against elastic fiber formation disorders, pharmacological manipulations of 3DCMs are essential. In this context, we examined whether elastic fiber formation in 3DCMs was regulated by the drug that inhibits the cross-linking of elastin monomers to form insoluble elastic fibers [1,26]. When BAPN, an inhibitor of LOX, was applied to 3DCMs for the last two days of culture, the elastic fiber formation was significantly inhibited (Fig. 4A–C).

The biosynthesis of PGE_2 is increased in human atherosclerotic plaques [36] and has been implicated in atherosclerotic plaque rupture [37]. PGE_2 is abundantly produced in aortic aneurysmal lesions and it decreases elastic fiber formation [38,39]. Therefore, we stimulated the 3DCMs with PGE_2 and found that PGE_2 stimulation induced a partial disruption of the layer structure of SMCs (Fig. 4D–E) and decreased elastic fiber formation (Fig. 4F–K). These data suggest the potential use of 3DCMs for pharmacological manipulation of elastic fiber formation.

3.5. Infiltration of macrophages decreased elastic fibers in 3DCMs

The infiltration of macrophages into the vascular wall is a critical step in the progression of atherosclerosis and aortic aneurysm, and macrophages are the main source of PGE_2. We applied THP-1 (human monocyte cell line) to the 3DCMs with or without PMA, which induces the differentiation of THP-1, into activated macrophages. Non-activated THP-1 (CTRL) did not infiltrate 3DCMs or affect the SMC layer structure or elastic fiber formation (Fig. 5A, C, E, and G). On the other hand, activated macrophages infiltrated the 3DCMs (Fig. 5D, H) and decreased the surrounding elastic fibers and disrupted the layer structure of SMCs (Fig. 5)B, F, H, and I.

4. Discussion

Despite numerous discoveries related to the molecular mechanisms of elastic fiber formation, circulatory diseases associated with elastic fiber disorder, such as aneurysms and atherosclerosis, remain the predominant cause of mortality and morbidity in the developed world [40]. No pharmacological strategy to restore the elastic fiber assembly in diseased vessels or to inhibit the progression of elastin-related diseases is currently available. To obtain further mechanistic insights into elastic fiber formation, in the current study, we sought to create a new experimental vascular model designed specifically for vascular elastic fiber research. We optimized culture conditions and found that 3DCMs consisting of fibronectin-gelatin-coated neonatal rat aortic SMCs cultured in 1% FBS/DMEM exhibited layered elastic fiber formation within seven days, and that the amount of newly synthesized insoluble elastic fibers was significantly greater in 3DCMs than in 2D-SMCs cultured in the same medium.

Recent advances in tissue-engineered blood vessels that are free of synthetic scaffolds enabled the assembly of multiple layers of SMCs and the production of elastic fiber deposition in vitro [41]. These techniques provide excellent mechanical properties as implantable vascular constructs but require an excessively long culturing time and/or an in vivo bioreactor, neither of which are practical for ex vivo experimental vascular models. In this study, fibronectin nanofilms prepared on the surface of SMCs, which has not been used in other tissue-engineered blood vessels, were adopted in 3DCMs for hierarchical cell manipulation and rapid induction of elastic fiber formation. The recent proteomics approach enabled comprehensive molecular interactions in elastic fiber assembly and revealed that fibronectin and microfibril fibrillin play a central role [42]. Kinsey et al. and Sabatier et al. demonstrated that, in addition to expression, fibronectin assembly is a prerequisite for fibrillin assembly [10,16]. It is noted that fibronectin assembly and subsequent fibrillin assembly in vitro were observed within a couple of days in the static culture condition [10,16]. Other lines of in vitro studies demonstrated that fibronectin is critical for the deposition of latent transforming growth factor β-binding protein-1 (LTBP-1), which is associated with microfibrils [11], and that fibronectin assembly promotes LOX activation [14]. Our previous report demonstrated that pericellular fibronectin fibers were observed in 3DCMs within 24 h [9]. In addition, our results demonstrated that the use of ε-poly(lysine) instead of fibronectin failed to generate elastic fiber formation. These data support our

1 mm. (F–G) EVG stain of 3DCMs. (H–I) Immunofluorescent images of fibrillin-1 in 3DCMs red: fibrillin-1. Scale bars: 50 μm. CTRL (D,F,H) and PGE_2 stimulation (E,G,I). (J) top panel: Histograms showing the density of EVG positive area/total area. lower panels: EVG stain of CTRL 3DCMs and PGE_2 stimulated 3DCMs. Scale bars: 100 μm. (K) Quantification of density of fibrillin-1 in (H) and (I). $n = 11$. $^*p < 0.05$.

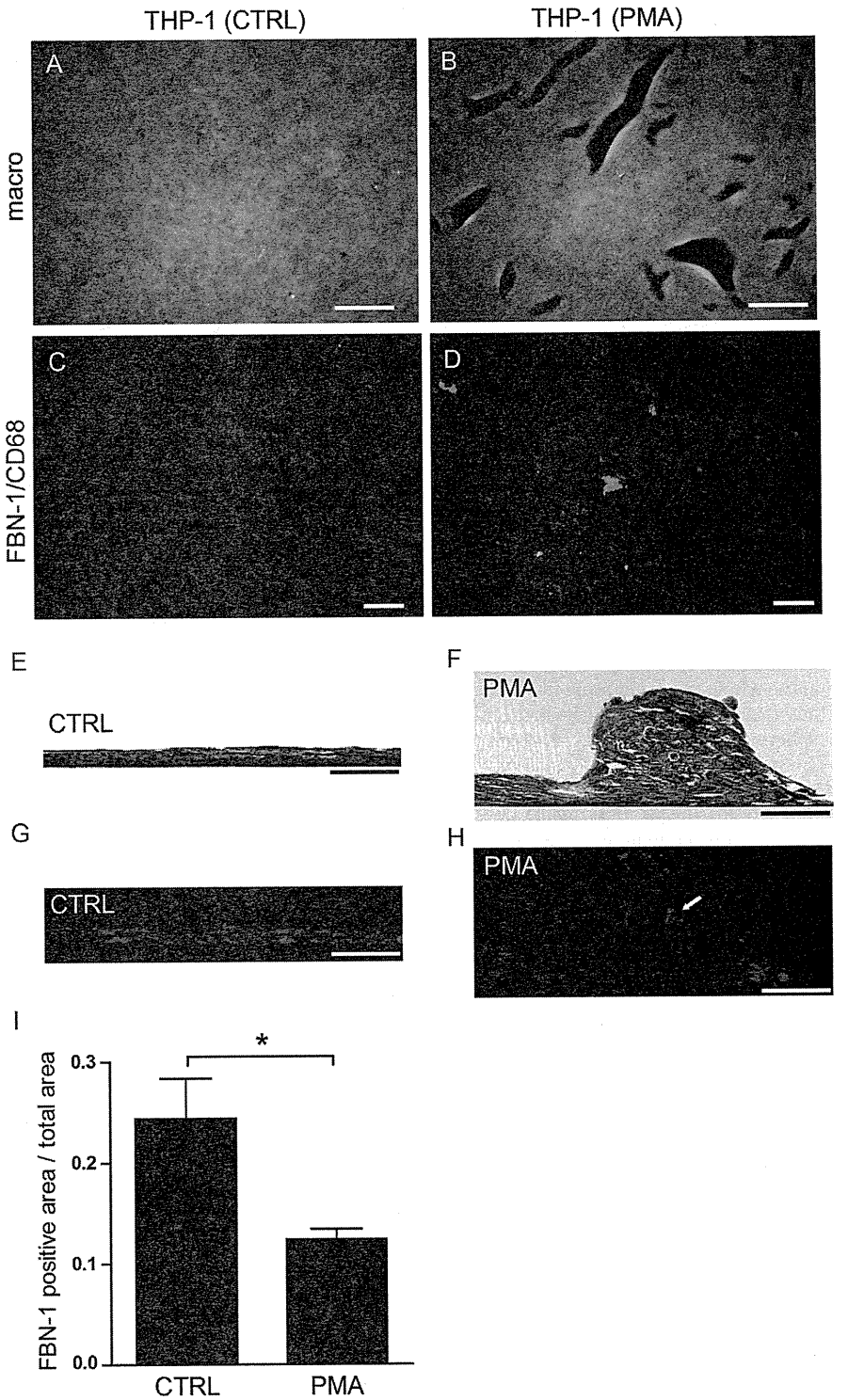

Fig. 5. Infiltration of macrophages decreased elastic fibers in 3DCMs (A–B) Macroscopic images of 3DCMs treated with non-activated THP-1 (CTRL), or activated macrophages (PMA). Scale bars: 1 mm. (C–D) Immunofluorescent images of fibrillin-1 (red) and CD68 (green) in 3DCMs. (E–F) EVG stain of 3DCMs. (G–H) Immunofluorescent image of fibrillin-1 (red) and CD 68 (green) in 3DCMs. White arrow indicates infiltrated macrophage. Scale bars: 50 μm. (I) Quantification of the density of fibrillin-1 in (G) and (H). $n = 11$. $^*p < 0.05$.

concept that the pericellular fibronectin meshwork on SMCs contributes to elastic fiber assembly in 3DCMs.

Elastin molecules play a crucial role in elastic fiber formation [1]. It has been reported that elastin is expressed maximally at the G_0 and minimally at the G_2/M phase during the cell cycle [43,44]. In accordance with previous reports, serum withdrawal increased tropoelastin mRNA expression in both 3DCMs and 2D-SMCs. Our data suggest that serum withdrawal–induced cell cycle regulation

has a favorable effect on elastic fiber formation. Fibrillin-2 which contributes to the initial assembly of elastic fibers as well as fibrillin-1 was also induced by serum-starved conditions in both 3DCMs and 2D-SMCs. Cell cycle regulation potentially contributes to the formation of elastic fibers in 3DCMs via the increase in elastin and fibrillin-2.

In addition to the fibronectin nanofilm and culture media component, the use of neonatal vascular SMCs may also contribute to elastic fiber formation in 3DCMs, because it has been well documented that adult vascular SMCs lose the ability to produce components related to elastic fiber assembly, including tropoelastin and fibrillins [1,22,24]. In our study, 3DCMs using adult human aortic SMCs did not produce elastic fibers, even if the same fibronectin coating and culture conditions were applied. In addition to these factors, our data suggest that a certain number of SMC layers are required for elastic fiber formation. Although the exact mechanisms of the rapid induction of elastic fibers in 3DCMs are not known, the multiple factors in 3DCMs, such as the type of SMC, the ECM coated on the cells, the culture media components, and the number of SMC layers are considered to allow layered elastic fibers even in short periods in a static culture condition.

Under physiological conditions, the majority of SMCs in the medial layer of the artery are considered to be in a differentiated (contractile) state that is hardly retained in planar cell culture [29]. Unexpectedly, our results suggest that SMC phenotypes in 3DCMs are similar to those in 2D-SMCs except SMemb expression. Since the differentiated status in SMCs varies through developmental stages and under pathological conditions, including atherosclerosis and vascular injury [45], an understanding of the differentiation status of SMCs in 3DCMs is important in vascular biology research. One study limitation is that SMCs in 3DCMs were not fully differentiated and the elasticity seemed significantly low compared to native vascular tissues. Further modification of 3DCMs, such as modulating SMC phenotypes before creating 3D construction by means of pharmacological stimuli or mechanical stress, is required in future studies.

In the present study, we demonstrated that elastic fiber formation in 3DCMs was disturbed by a LOX inhibitor and PGE_2, suggesting that pharmacological manipulation could be applied in 3DCMs. The relatively small reduction in elastic fiber formation by BAPN may be due to the 2-day administration out of the 7 days of culture. In conventional in vivo study using systemic drug administration, drug metabolism profoundly affects it efficacy, and its indirect effects cannot be discriminated. Although emerging evidence has demonstrated advances in drug delivery systems such as nanoparticles and antibody-drug conjugates that enable tissue-specific targeting strategy, they remain impractical for initial drug screening [46]. 3DCMs may offer a new strategy to examine the direct effects of various drugs on vascular elastic fiber formation and phenotypic changes of SMCs.

There have been excellent in vitro systems using 2D culture to examine molecular mechanisms of elastic fiber formation [5–7], because insoluble mature elastic fibers can be formed in certain conditions of 2D culture systems. However, elastic fiber formation in a vertical sectional view cannot be observed in 2D culture systems. In this study, it is suggested that the infiltration of macrophages and its effects on the spatial arrangement of elastic fibers can be observed in 3DCMs.

Spheroid culture system has been established as a 3D culture of SMCs. For example, the spheroids with vascular SMCs retain electrophysiological and contractile properties [47,48]. Paracrine effects of SMCs on gap junction formation of endothelial cells were also shown using the spheroids with human vascular cells [49]. To the best of our knowledge, however, elastic fiber formation and the effect of macrophage infiltration on SMCs have not been reported in SMC spheroids. Our study revealed that, in SMC spheroids, a few numbers of elastic laminae were formed between the outer shell and porous core at least under the same culture conditions as 3DCMs. Since a single spheroid has around 100 μm in diameter and consists of heterogeneous SMC phenotypes (Supplemental Fig. 5), it seems difficult to construct larger numbers of elastic laminae. On the other hand, the 3DCMs exhibited multiple layered elastic laminae spread over an area of at least 5 mm^2 (Fig. 4D). Furthermore, it was visible with a low magnification that macrophage infiltration induced disruption of elastic fiber assembly in the 3DCMs. In comparison with spheroid culture system, 3DCMs would be suitable for studies of elastic fiber formation in pathophysiological setting.

In conclusion, 3DCMs have the potential to be a new vascular experimental platform in which the spatial and temporal regulation of vascular elastic fibers can be observed. Since the regulation of vascular elastic fiber formation can be examined in 3DCMs, they may be useful for exploring pharmacological therapeutic strategies against disordered elastic fiber homeostasis, such as atherosclerotic vascular disease for which no pharmacological treatment is currently available.

Funding sources

This work was supported by grants from the Ministry of Education, Culture, Sports, Science and Technology of Japan (U.Y., Y. Ichikawa, S.M., Y. Ishikawa.), the Grant-in-Aid for Scientific Research on Innovative Areas (UY, 1123116514; Y. Ishikawa, 22136009), the Ministry of Health, Labour and Welfare (Y. Ishikawa), the Grant-in-Aid for Scientific Research (S) from the Japan Society for the Promotion of Science (JSPS)(M.A.), the NEXT Program from JSPS (M.M., LR026) the National Cerebral and Cardiovascular Center (Y. Ishikawa), the Yokohama Foundation for Advanced Medical Science (U.Y.), the Vehicle Racing Commemorative Foundation (U.Y., S.M.), and the Takeda Science Foundation (U.Y., S.M.).

Disclosures

No disclosure.

Acknowledgments

We are grateful to Yuka Sawada for the excellent technical assistance.

Appendix A. Supplementary data

Supplementary data related to this article can be found at http://dx.doi.org/10.1016/j.atherosclerosis.2014.01.045.

References

[1] Wagenseil JE, Mecham RP. Vascular extracellular matrix and arterial mechanics. Physiol Rev 2009;89:957–89.
[2] Cheng KS, Baker CR, Hamilton G, et al. Arterial elastic properties and cardiovascular risk/event. Eur J Vasc Endovasc Surg 2002;24:383–97.
[3] Liu C, Zheng D, Zhao L, et al. Elastic properties of peripheral arteries in heart failure patients in comparison with normal subjects. J Physiol Sci 2013;63:195–201.
[4] Nakamura T, Ruiz-Lozano P, Lindner V, et al. DANCE, a novel secreted RGD protein expressed in developing, atherosclerotic, and balloon-injured arteries. J Biol Chem 1999;274:22476–83.
[5] Yeo GC, Baldock C, Tuukkanen A, et al. Tropoelastin bridge region positions the cell-interactive C terminus and contributes to elastic fiber assembly. Proc Natl Acad Sci U S A 2012;109:2878–83.

[6] Wachi H, Sato F, Murata H, et al. Development of a new in vitro model of elastic fiber assembly in human pigmented epithelial cells. Clin Biochem 2005;38:643–53.
[7] Faris B, Jackson LE, Schreiber BM, et al. A controlled precursor add-back model of elastogenesis in smooth muscle cell cultures. Matrix 1991;11:367–72.
[8] Matsusaki M, Kadowaki K, Nakahara Y, et al. Fabrication of cellular multilayers with nanometer-sized extracellular matrix films. Angew Chem Int Ed Engl 2007;46:4689–92.
[9] Matsusaki M, Kadowaki K, Adachi E, et al. Morphological and histological evaluations of 3D-layered blood vessel constructs prepared by hierarchical cell manipulation. J Biomater Sci Polym Ed 2012;23:63–79.
[10] Kinsey R, Williamson MR, Chaudhry S, et al. Fibrillin-1 microfibril deposition is dependent on fibronectin assembly. J Cell Sci 2008;121:2696–704.
[11] Dallas SL, Sivakumar P, Jones CJ, et al. Fibronectin regulates latent transforming growth factor-beta (TGF beta) by controlling matrix assembly of latent TGF beta-binding protein-1. J Biol Chem 2005;280:18871–80.
[12] Sottile J, Shi F, Rublyevska I, et al. Fibronectin-dependent collagen I deposition modulates the cell response to fibronectin. Am J Physiol Cell Physiol 2007;293:C1934–46.
[13] Velling T, Risteli J, Wennerberg K, et al. Polymerization of type I and III collagens is dependent on fibronectin and enhanced by integrins alpha 11beta 1 and alpha 2beta 1. J Biol Chem 2002;277:37377–81.
[14] Fogelgren B, Polgar N, Szauter KM, et al. Cellular fibronectin binds to lysyl oxidase with high affinity and is critical for its proteolytic activation. J Biol Chem 2005;280:24690–7.
[15] Wierzbicka-Patynowski I, Schwarzbauer JE. The ins and outs of fibronectin matrix assembly. J Cell Sci 2003;116:3269–76.
[16] Sabatier L, Chen D, Fagotto-Kaufmann C, et al. Fibrillin assembly requires fibronectin. Mol Biol Cell 2009;20:846–58.
[17] Yokoyama U, Minamisawa S, Quan H, et al. Chronic activation of the prostaglandin receptor EP4 promotes hyaluronan-mediated neointimal formation in the ductus arteriosus. J Clin Invest 2006;116:3026–34.
[18] Yokoyama U, Minamisawa S, Adachi-Akahane S, et al. Multiple transcripts of Ca2+ channel alpha1-subunits and a novel spliced variant of the alpha1C-subunit in rat ductus arteriosus. Am J Physiol Heart Circ Physiol 2006;290:H1660–70.
[19] Jin MH, Yokoyama U, Sato Y, et al. DNA microarray profiling identified a new role of growth hormone in vascular remodeling of rat ductus arteriosus. J Physiol Sci 2011;61:167–79.
[20] Hirai M, Ohbayashi T, Horiguchi M, et al. Fibulin-5/DANCE has an elastogenic organizer activity that is abrogated by proteolytic cleavage in vivo. J Cell Biol 2007;176:1061–71.
[21] Yokoyama U, Minamisawa S, Shioda A, et al. Prostaglandin E2 inhibits elastogenesis in the ductus arteriosus via EP4 signaling. Circulation 2013;129: 487–96.
[22] Kelleher CM, McLean SE, Mecham RP. Vascular extracellular matrix and aortic development. Curr Top Dev Biol 2004;62:153–88.
[23] Wagenseil JE, Mecham RP. New insights into elastic fiber assembly. Birth Defects Res C Embryo Today 2007;81:229–40.
[24] McMahon MP, Faris B, Wolfe BL, et al. Aging effects on the elastin composition in the extracellular matrix of cultured rat aortic smooth muscle cells. Vitro Cell Dev Biol 1985;21:674–80.
[25] Long JL, Tranquillo RT. Elastic fiber production in cardiovascular tissue-equivalents. Matrix Biol 2003;22:339–50.
[26] Kagan HM, Li W. Lysyl oxidase: properties, specificity, and biological roles inside and outside of the cell. J Cell Biochem 2003;88:660–72.
[27] Hirai M, Horiguchi M, Ohbayashi T, et al. Latent TGF-beta-binding protein 2 binds to DANCE/fibulin-5 and regulates elastic fiber assembly. EMBO J 2007;26:3283–95.
[28] Horiguchi M, Inoue T, Ohbayashi T, et al. Fibulin-4 conducts proper elastogenesis via interaction with cross-linking enzyme lysyl oxidase. Proc Natl Acad Sci U S A 2009;106:19029–34.
[29] Owens GK, Kumar MS, Wamhoff BR. Molecular regulation of vascular smooth muscle cell differentiation in development and disease. Physiol Rev 2004;84: 767–801.
[30] Aikawa M, Sivam PN, Kuro-o M, et al. Human smooth muscle myosin heavy chain isoforms as molecular markers for vascular development and atherosclerosis. Circ Res 1993;73:1000–12.
[31] Glukhova MA, Kabakov AE, Frid MG, et al. Modulation of human aorta smooth muscle cell phenotype: a study of muscle-specific variants of vinculin, caldesmon, and actin expression. Proc Natl Acad Sci U S A 1988;85:9542–6.
[32] Shanahan CM, Cary NR, Metcalfe JC, et al. High expression of genes for calcification-regulating proteins in human atherosclerotic plaques. J Clin Invest 1994;93:2393–402.
[33] Kocher O, Gabbiani G. Cytoskeletal features of normal and atheromatous human arterial smooth muscle cells. Hum Pathol 1986;17:875–80.
[34] Kamijima T, Isobe M, Suzuki J, et al. Enhanced embryonic nonmuscle myosin heavy chain isoform and matrix metalloproteinase expression in aortic abdominal aneurysm with rapid progression. Cardiovasc Pathol 1999;8: 291–5.
[35] Jiao L, Xu Z, Xu F, et al. Vascular smooth muscle cell remodelling in elastase-induced aortic aneurysm. Acta Cardiol 2010;65:499–506.
[36] Cipollone F, Fazia ML, Iezzi A, et al. Association between prostaglandin E receptor subtype EP4 overexpression and unstable phenotype in atherosclerotic plaques in human. Arterioscler Thromb Vasc Biol 2005;25:1925–31.
[37] Linton MF, Fazio S. Cyclooxygenase products and atherosclerosis. Drug Discov Today Ther Strateg 2008;5:25–36.
[38] Walton LJ, Franklin IJ, Bayston T, et al. Inhibition of prostaglandin E2 synthesis in abdominal aortic aneurysms: implications for smooth muscle cell viability, inflammatory processes, and the expansion of abdominal aortic aneurysms. Circulation 1999;100:48–54.
[39] Yokoyama U, Ishiwata R, Jin MH, et al. Inhibition of EP4 signaling attenuates aortic aneurysm formation. PLoS One 2012;7:e36724.
[40] Lloyd-Jones D, Adams RJ, Brown TM, et al. Heart disease and stroke statistics–2010 update: a report from the American Heart Association. Circulation 2010;121:e46–215.
[41] Peck M, Gebhart D, Dusserre N, et al. The evolution of vascular tissue engineering and current state of the art. Cells Tissues Organs 2012;195: 144–58.
[42] Cain SA, McGovern A, Small E, et al. Defining elastic fiber interactions by molecular fishing: an affinity purification and mass spectrometry approach. Mol Cell Proteomics 2009;8:2715–32.
[43] Wachi H, Seyama Y, Yamashita S, et al. Cell cycle-dependent regulation of elastin gene in cultured chick vascular smooth-muscle cells. Biochem J 1995;309(Pt 2):575–9.
[44] Seyama Y, Wachi H. Atherosclerosis and matrix dystrophy. J Atheroscler Thromb 2004;11:236–45.
[45] Aikawa M, Yamaguchi H, Yazaki Y, et al. Smooth muscle phenotypes in developing and atherosclerotic human arteries demonstrated by myosin expression. J Atheroscler Thromb 1995;2:14–23.
[46] Lobatto ME, Fuster V, Fayad ZA, et al. Perspectives and opportunities for nanomedicine in the management of atherosclerosis. Nat Rev Drug Discov 2011;10:835–52.
[47] Gentile C, Fleming PA, Mironov V, et al. VEGF-mediated fusion in the generation of uniluminal vascular spheroids. Dev Dyn 2008;237:2918–25.
[48] Harder DR, Sperelakis N. Action potential generation in reaggregates of rat aortic smooth muscle cells in primary culture. Blood Vessels 1979;16:186–201.
[49] Korff T, Kimmina S, Martiny-Baron G, et al. Blood vessel maturation in a 3-dimensional spheroidal coculture model: direct contact with smooth muscle cells regulates endothelial cell quiescence and abrogates VEGF responsiveness. FASEB J 2001;15:447–57.

OPEN ACCESS Freely available online

PLOS | ONE

Store-Operated Ca^{2+} Entry (SOCE) Regulates Melanoma Proliferation and Cell Migration

Masanari Umemura[1]*, Erdene Baljinnyam[2], Stefan Feske[3], Mariana S. De Lorenzo[2], Lai-Hua Xie[2], Xianfeng Feng[1], Kayoko Oda[1], Ayako Makino[1], Takayuki Fujita[1], Utako Yokoyama[1], Mizuka Iwatsubo[2], Suzie Chen[4], James S. Goydos[5], Yoshihiro Ishikawa[1], Kousaku Iwatsubo[1,2]*

1 Cardiovascular Research Institute, Yokohama City University School of Medicine, Yokohama, Japan, **2** Department of Cell Biology and Molecular Medicine, New Jersey Medical School, Rutgers, The State University of New Jersey, Newark, New Jersey, United States of America, **3** Department of Pathology, New York University School of Medicine, New York, New York, United States of America, **4** Department of Chemical Biology, Susan Lehman Cullen Laboratory of Cancer Research in the Ernest Mario School of Pharmacy, Rutgers, The State University of New Jersey, Piscataway, New Jersey, United States of America, **5** Division of Surgical Oncology, Department of Surgery, Robert Wood Johnson Medical School, Rutgers, The State University of New Jersey, Piscataway, New Jersey, United States of America

Abstract

Store-operated Ca^{2+} entry (SOCE) is a major mechanism of Ca^{2+} import from extracellular to intracellular space, involving detection of Ca^{2+} store depletion in endoplasmic reticulum (ER) by stromal interaction molecule (STIM) proteins, which then translocate to plasma membrane and activate Orai Ca^{2+} channels there. We found that STIM1 and Orai1 isoforms were abundantly expressed in human melanoma tissues and multiple melanoma/melanocyte cell lines. We confirmed that these cell lines exhibited SOCE, which was inhibited by knockdown of STIM1 or Orai1, or by a pharmacological SOCE inhibitor. Inhibition of SOCE suppressed melanoma cell proliferation and migration/metastasis. Induction of SOCE was associated with activation of extracellular-signal-regulated kinase (ERK), and was inhibited by inhibitors of calmodulin kinase II (CaMKII) or Raf-1, suggesting that SOCE-mediated cellular functions are controlled via the CaMKII/Raf-1/ERK signaling pathway. Our findings indicate that SOCE contributes to melanoma progression, and therefore may be a new potential target for treatment of melanoma, irrespective of whether or not Braf mutation is present.

Citation: Umemura M, Baljinnyam E, Feske S, De Lorenzo MS, Xie L-H, et al. (2014) Store-Operated Ca^{2+} Entry (SOCE) Regulates Melanoma Proliferation and Cell Migration. PLoS ONE 9(2): e89292. doi:10.1371/journal.pone.0089292

Editor: Laszlo Csernoch, University of Debrecen, Hungary

Received May 29, 2013; **Accepted** January 21, 2014; **Published** February 21, 2014

Copyright: © 2014 Umemura et al. This is an open-access article distributed under the terms of the Creative Commons Attribution License, which permits unrestricted use, distribution, and reproduction in any medium, provided the original author and source are credited.

Funding: This study was supported by the American Heart Association (SDG 0835596D) and by the Foundation of UMDNJ and by the Melanoma Research Foundation (K. Iwatsubo). This study was also supported by the Japan Heart Foundation and by the Kanagawa Nanbyo Foundation (M. Umemura). This study was supported in part by the Ministry of Health, Labor and Welfare, a Grant-in-Aid for Scientific Research on Innovative Areas (22136009), and the Japanese Ministry of Education, Culture, Sports, Science, and Technology (Y. Ishikawa). The funders had no role in study design, data collection and analysis, decision to publish, or preparation of the manuscript.

Competing Interests: The authors have declared that no competing interests exist.

* E-mail: iwatuko@njms.rutgers.edu (KI); umemurma@yokohama-cu.ac.jp (MU)

Introduction

Melanoma has the poorest prognosis among skin cancers, although drugs targeting aberrant ERK signaling, i.e., mutated serine/threonine-protein kinase Braf, have improved both overall and progression-free survival times [1]. However, this therapy is not effective in patients without Braf mutation, and some patients with Braf mutation rapidly acquire resistance to Braf inhibitors [2]. Accordingly, a different approach to target ERK signaling regardless of Braf mutation is needed.

Intracellular Ca^{2+} signaling regulates diverse cellular functions including proliferation and cell migration [3]. Store-operated Ca^{2+} entry (SOCE) is a major mechanism of Ca^{2+} import from extracellular to intracellular space, especially in non-excitable cells [4]. In general, activation of inositol 1,4,5-trisphosphate (IP_3) receptors on the endoplasmic reticulum (ER) evokes a rapid and transient release of Ca^{2+} from the ER store. The resulting decrease of Ca^{2+} concentration in the ER is sensed by the EF-hand motif of stromal interaction molecules (STIM), which then translocate to the plasma membrane, where they interact with Orai Ca^{2+} channel subunits [5], leading to Ca^{2+} influx from extracellular space to restore the Ca^{2+} concentration in ER [6].

The physiological functions of STIM and Orai have been studied mainly in connection with the immune system [7–10]. Orai channels control Ca^{2+} release-activated Ca^{2+} (CRAC) currents in lymphocytes [4], and also contribute to SOCE currents in other types of cells, such as endothelial cells [11]. STIM1 and Orai1, but not STIM2, Orai2 or Orai3, have roles in cell migration of smooth muscle cells [12,13]. Examination of a library of randomized ribozymes indicated that STIM1 is a metastasis-related gene [14]. SOCE is involved in proliferation, cell migration, and angiogenesis in cervical cancer [15], and cell migration in breast cancer [16]. However, the role of SOCE in melanoma has been little investigated, except for a recent paper demonstrating Akt signaling activation in mouse melanoma cells, especially in lipid rafts [17]. In the present study, we show that SOCE promotes melanoma progression by enhancing cell proliferation, migration, and metastasis through activation of ERK signaling via the CaMKII/Raf-1/ERK pathway.

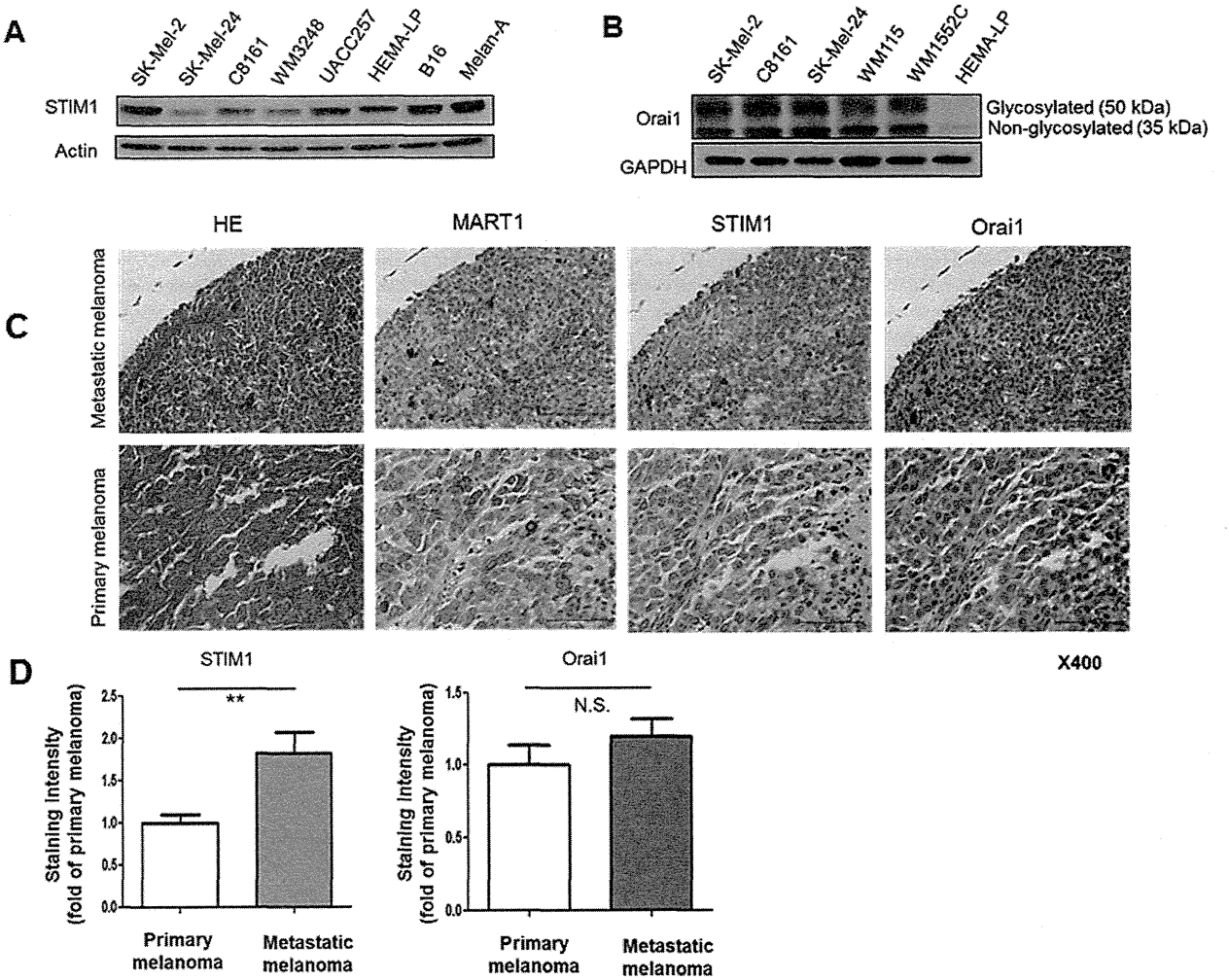

Figure 1. Expression of STIM1 and Orai1 in melanoma. (**A and B**) Western blot analyses of STIM1 (A) and Orai1 (B) expression in the indicated cell lines. (**C**) Immunohistochemical stainings of HE, MART1, STIM1 (the antibody from Abnova was used) and Orai1 (the antibody from Sigma was used) in a melanoma tissue microarray (original magnification, x400). Calibration bars represent 100 μm. (**D**) Analyses of the staining intensity of expression of STIM1 and Orai1. *, $p<0.05$; **, $p<0.01$, n = 8.
doi:10.1371/journal.pone.0089292.g001

Materials and Methods

Reagents and Cell Lines

Reagents were purchased from Sigma unless otherwise specified. Antibodies to β-actin, GAPDH, and ERK were purchased from Santa Cruz. α-Spectrin antibody was purchased from Millipore. Phospho-ERK antibody was purchased from Cell Signaling. Antibodies against STIM1 were purchased from BD Transduction Laboratories and Abnova [18]. Antibodies against Orai1 were previously generated by us [19], or purchased from Sigma [12]. Second antibodies for mouse and rabbit were purchased from Abcam and Cell Signaling, respectively. GW5074 was purchased from Focus Biomolecules. W5 hydrochloride was purchased from Tokyo Chemical Industry. GDC-0879 was purchased from Selleckhem [20]. SK-Mel-2 and SK-Mel-24 (human metastatic melanoma) cell lines were obtained from the American Type Culture Collection. UACC257 (human metastatic melanoma) was obtained from the Charles River Laboratory. Melan-A mouse melanocyte cell line was purchased from Welcome Trust Functional Genomics Cell Bank, St. George's, University of London. C8161 cell line was kindly provided by Dr. Mary J.C. Hendrix. WM3248 and WM115 (primary melanoma, vertical growth phase (VGP)) and WM1552C (primary melanoma, radial growth phase (RGP)) cell lines were kindly provided by Dr. Meenhard Herlyn. HEMA-LP (human melanocyte) cell line was obtained from Invitrogen. SK-Mel-2 and SK-Mel-24 cells were maintained in MEM containing 10% fetal bovine serum (FBS) and 1% penicillin-streptomycin. UACC257 cells were maintained in RPMI-1640 (Sigma) containing 10% FBS and 1% penicillin-streptomycin. HEMA-LP was maintained in an EndoGRO-VEGF Complete media kit (Millipore). All other melanoma cells were maintained in RPMI (Gibco) containing 10% FBS and 1% penicillin-streptomycin.

Western Blot Analysis

Western blot analyses were performed as we previously described [21]. Briefly, cells were lysed and sonicated in RIPA buffer (Thermo Scientific). Equal amounts of protein were subjected to sodium dodecyl sulfate polyacrylamide gel electro-

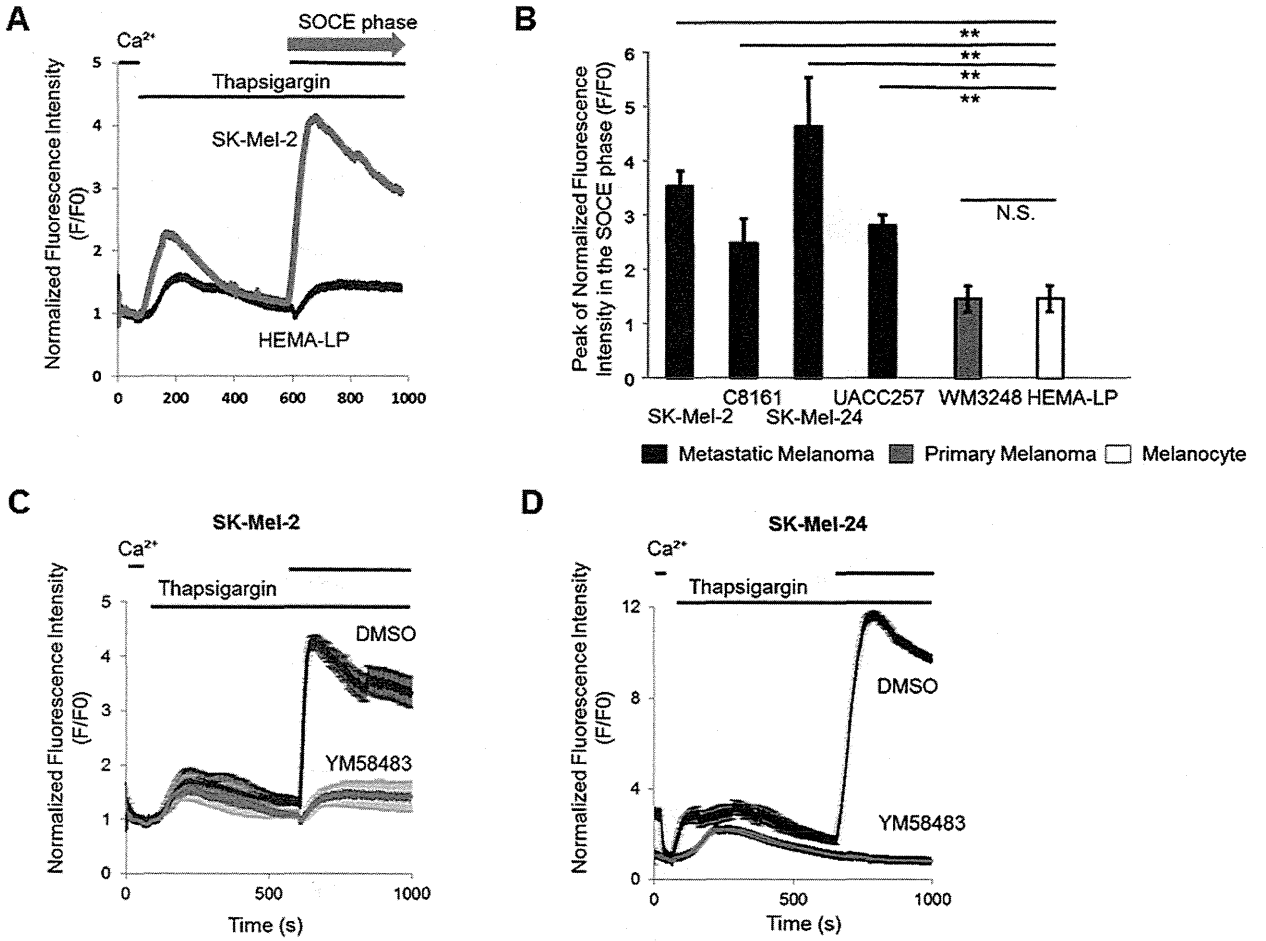

Figure 2. SOCE occurs in melanoma. (**A**) Cytosolic Ca^{2+} levels in SK-Mel-2 cells. Extracellular Ca^{2+} (2 mM) was removed, followed by the addition of thapsigargin (TG) (2 μM) for Ca^{2+} depletion in the ER. Ca^{2+} (2 mM) was then added to the extracellular fluid, and SOCE-induced Ca^{2+} elevation was observed (SOCE phase). (**B**) Ca^{2+} peak amplitude in the SOCE phase was compared among melanoma and melanocyte cell lines. **, $p<0.01$ (HEMA-LP), n = 6–8. (**C and D**) Cytosolic Ca^{2+} levels in SK-Mel-2 and SK-Mel-24 cells are shown as means ± SD (n = 6–10). SOCE was examined in the presence or absence of DMSO (1 μM) or YM58483 (1 μM) in SK-Mel-2 (**C**) and SK-Mel-24 cells (**D**).
doi:10.1371/journal.pone.0089292.g002

phoresis (SDS-PAGE). After protein separation by electrophoresis, samples were transferred to Millipore Immobilon-P membrane followed by immunoblotting with antibodies against molecules of interest. Immunoblottings for STIM1 and Orai1 were performed with the antibodies from BD Transduction Laboratories and from Sigma, respectively. Signal intensities of bands were quantified with Image J software (NIH).

Immunohistochemistry

Immunohistochemical stainings were performed as we previously described [22]. Melanoma tissue microarray plates (US Biomax Cat. #T085 and #ME1004a) were subjected to immunohistochemistry with antibodies against melanoma antigen recognized by T-cells 1 (MART1) (Millipore), STIM1 and Orai1. Two different antibodies against STIM1 (purchased from BD Transduction Laboratories and Abnova) and Orai1 (generated by us [19] and purchased from Sigma) were used to confirm the specificity of the staining. Negative control samples were exposed to the secondary antibody alone. Quantification of STIM1 expression was performed with BZ-II analyzer software (Keyence) as we previously described [23].

Fluorescence Imaging of Intracellular Ca^{2+}

Measurement of intracellular Ca^{2+} level was performed as we previously described [24]. Cells were incubated with 2-[4-(2-hydroxyethyl)-1-piperazinyl]ethanesulfonic acid (HEPES) buffer containing 4 μmol/l of Fluo-4AM, followed by washing and incubation with HEPES-buffered saline containing 2.0 mmol/L of $CaCl_2$. An iXon+885 charge-coupled-device camera (Andor Technology) was used to monitor fluorescence changes. Full images were collected every 4 s. Fluo-4 fluorescence was excited at 488 nm, and data were expressed as normalized changes in background-corrected fluorescence emission (F/F_0). Data were analyzed using Imaging Workbench (INDEC BioSystems). Representative Ca^{2+} signals averaged from 6 to 10 individual cells are shown in the figures.

Transduction of Short Hairpin RNA (shRNA)

SK-Mel-2, SK-Mel-24 and C8161 cells were transduced with STIM1 shRNA, Orai1 shRNA, and scramble control shRNA using lentivirus (Santa Cruz Biotechnology) according to the protocols provided by the manufacturer. Briefly, cells were incubated with 10 μg/mL of Polybrene (Santa Cruz Biotechnol-

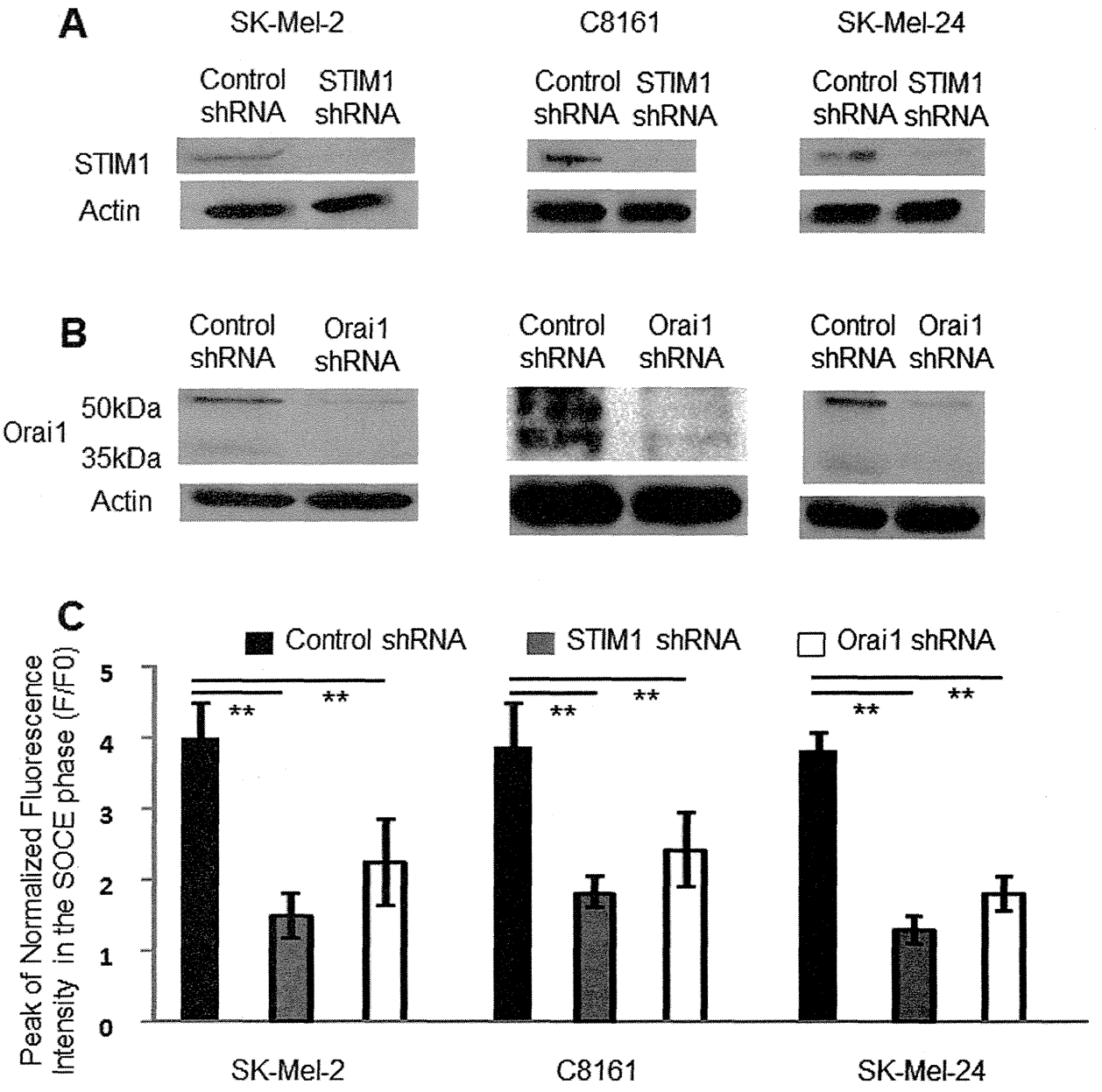

Figure 3. SOCE was inhibited by STIM1- or by Orai1-knockdown in melanoma cell lines. (**A and B**) Western blot analyses of protein expressions of STIM1 (A) and Orai1 (B) in metastatic melanoma cell lines. shRNA transduction reduced expression of the target proteins. (**C**) Ca^{2+} peak amplitude of SOCE was reduced by STIM1- or Orai1-knockdown. **, $p<0.01$, n = 6–10.
doi:10.1371/journal.pone.0089292.g003

ogy) and lentiviral particles harboring each shRNA, then selected with puromycin dihydrochloride (Santa Cruz Biotechnology) for 1 week. Puromycin-containing medium was replaced with fresh medium every 3 to 4 days.

3-(4,5-Dimethylthiazol-2-yl)-2,5-diphenyltetrazolium Bromide (MTT) Assay

Cells were seeded in a 96-well plate at 5,000 or 10,000 cells per well and cultured for 24 h. Viable cells were determined daily using the MTT Cell Proliferation Assay kit (ATCC) according to the manufacturer's instructions.

Apoptosis Assays

Apoptosis assays were performed as previously described [25]. Cells were seeded on 6 cm dishes, and incubated for 24 or 48 hours. Cells were washed twice with cold PBS, and transferred into culture tubes. Annexin V, allophycocyanin conjugate (APC) and 7-amino-actinomycin D (7-AAD) (BD Biosciences, California, U.S.A.) were then added to the tubes. Cells were incubated for 15 min at RT (25°C) in darkness, followed by FACS analysis (Canto^{TM} II, Japan Becton, Dickinson and Company, Tokyo, Japan) within 1 hour.

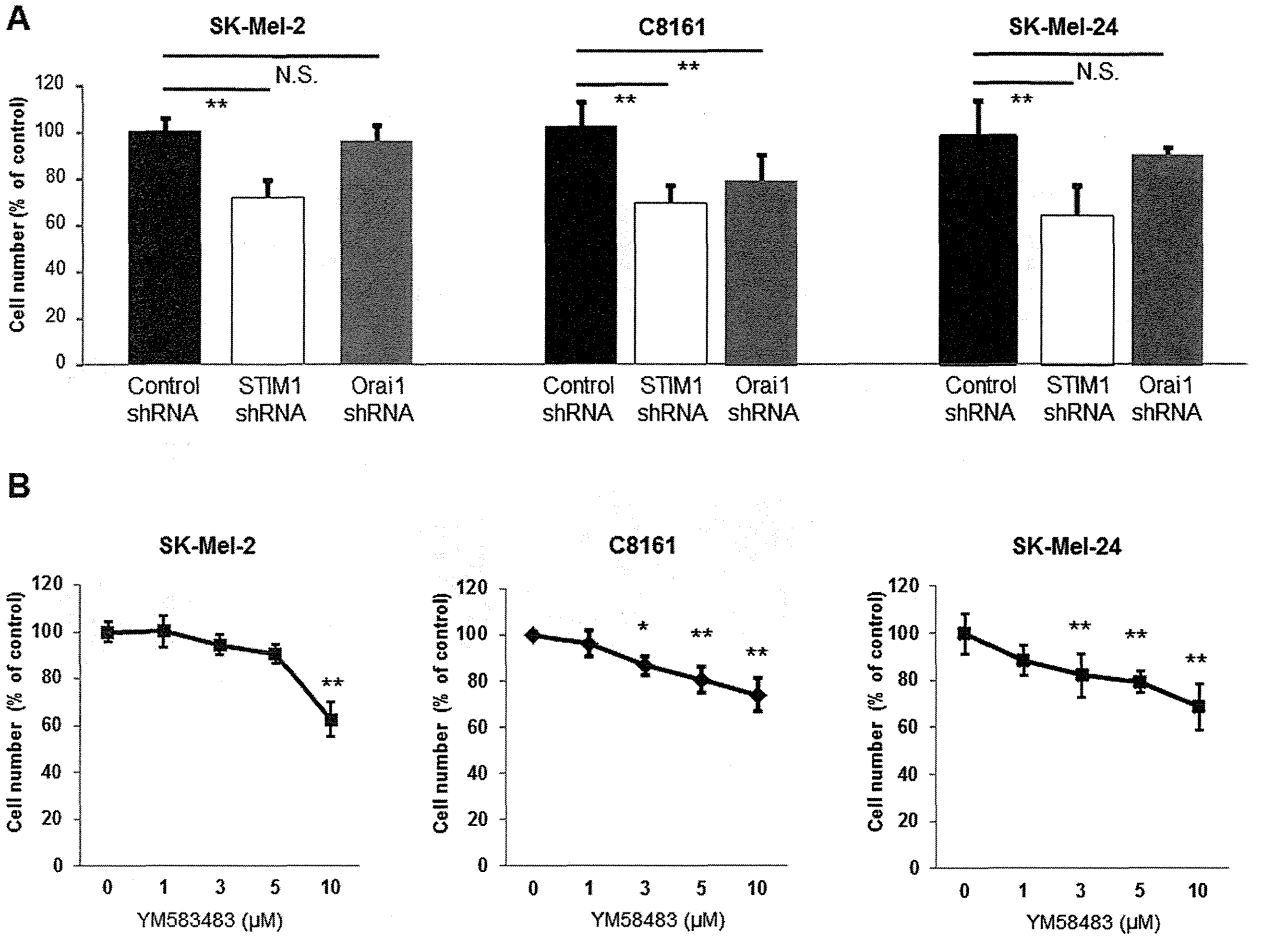

Figure 4. SOCE regulates proliferation of melanoma cells. (**A**) MTT assay of metastatic melanoma cell lines with or without STIM1- or Orai1-knockdown. **, $p<0.01$, n = 8. Representative data of 3 independent experiments are shown. (**B**) MTT assay of the indicated cell lines in the presence or absence of YM58483. *, $p<0.05$; **, $p<0.01$, n = 8. Representative data of 3 independent experiments are shown.
doi:10.1371/journal.pone.0089292.g004

Migration Assays

Migration assays were performed using 24-well Boyden chambers (8 μm pores, BD Biosciences) as we previously described [25]. The cells were plated at a density of 1×10^5 cells/100 μl of medium in the inserts, and incubated for 3 h at 37°C, followed by staining using a Diff-Quick kit (SIMENS). Pictures were taken with a microscope to count the number of migrated cells. The scratch wound method was also employed in some experiments as follows. Cells were seeded and allowed to form a monolayer for 24 h. The dish was scraped with the tip of a 100 μl pipette, and the resulting wound was washed with PBS two times [12]. Culture medium containing 10% FBS was added to the cells, and the cells were incubated at 37°C in 5% CO_2. Bright-field images were captured (Olympus IX51 microscope) and analyzed (Adobe Photoshop). The total number of pixels in empty spaces inside the wound were counted and normalized to the control.

Time-lapse Videomicroscopy

Analysis of cell motility using time-lapse videomicroscopy was performed as we previously described [25]. SK-Mel-2 cells were subjected to time-lapse video recording. Frames from the recording were digitized at 15-min intervals. Moving distance of each cell was analyzed by Image J software (NIH).

Calpain Activity Assay

Calpain activity was performed as previously described [26] with the calpain activity kit (Abcam) according to the manufacturer's instructions.

Immunocytochemistry

Immunocytochemistry was performed as previously described [24]. Filamentous actin (F-actin) staining was performed by incubation with rhodamine phalloidin (Invitrogen). Photographs were taken with a digital camera on a Nikon Eclipse TE200, and cells with one lamellipodium or more were counted manually.

Lung Colonization Assay

Lung colonization assay was performed as we previously described [22]. Cells were harvested and injected (2×10^6 cells/0.2 ml) into the tail veins of BALB/c nude mice (Charles River, male, 8 weeks old). Three weeks after the injection, metastatic colonies on the surface of the lungs were fixed with picric acid and counted under a dissection microscope.

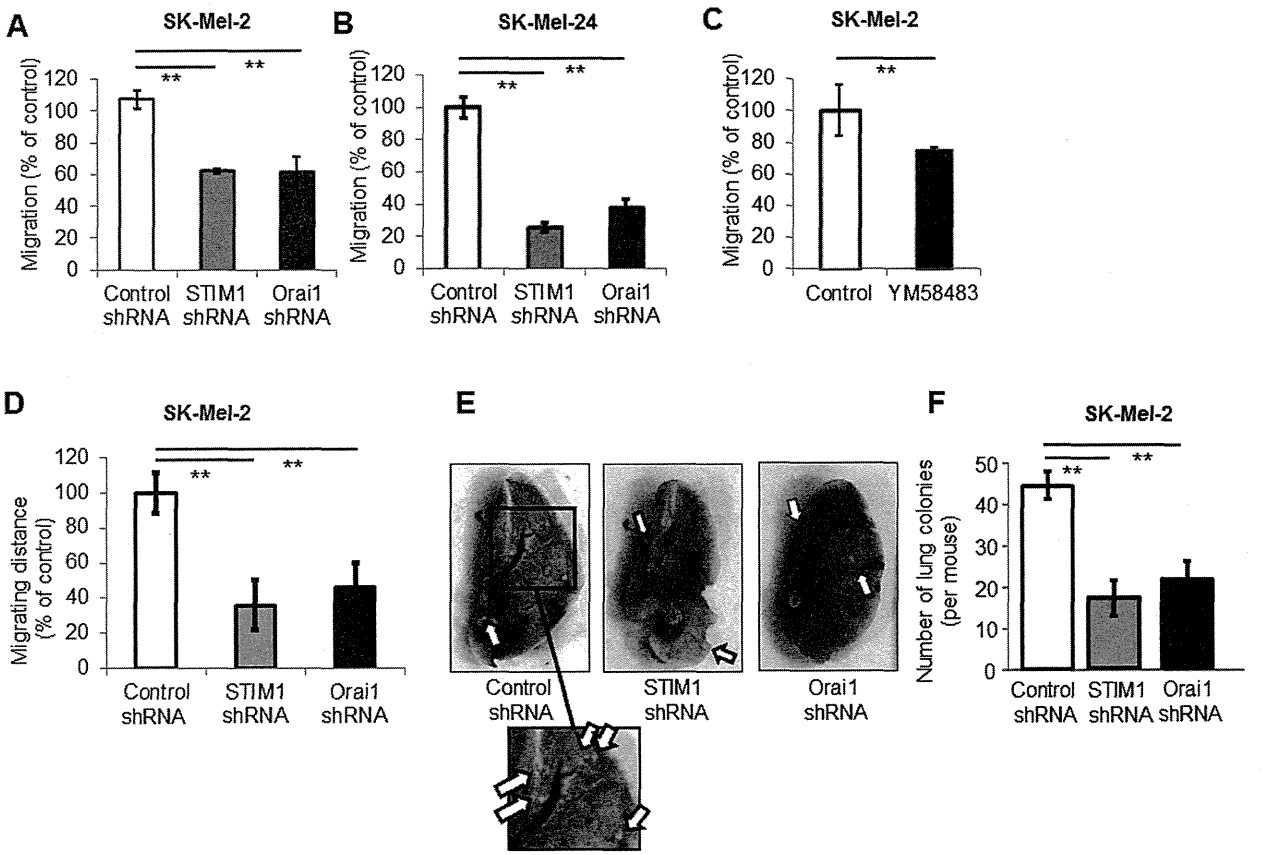

Figure 5. SOCE regulates cell migration and metastasis of melanoma. (**A and B**) Boyden chamber assay showed that either STIM1- or Orai1-knockdown inhibited cell migration. **, $p<0.01$, n = 4. (**C**) The scratch test showed that YM583483 (1 μM) inhibited cell migration. **, $p<0.01$, n = 4. (**D**) Time-lapse video recording (Videos S1, S2, and S3) showed that STIM1- or Orai1-knockdown SK-Mel-2 cells exhibited a shorter migration distance than control SK-Mel-2 cells. **, $p<0.01$, n = 10. (**E and F**) SK-Mel-2 cells with knockdown of either STIM1 or Orai1 were injected to the tail vein of Balb/c nu/nu mice. Three weeks later, the lungs were removed and fixed with picric acid. (**E**) Representative images of lung surface are shown. Arrows indicate metastatic melanoma colonies (white lesions). (**F**) The number of metastatic colonies in the lung surface was counted under a dissection microscope. **, $p<0.01$, n = 8.
doi:10.1371/journal.pone.0089292.g005

Data Analysis and Statistics

Statistical comparisons among groups were performed using Student's *t*-test or one-factor analysis of variance (ANOVA) with the Bonferroni post hoc test. The criterion of statistical significance was set at $p<0.05$. *, $p<0.05$, **, $p<0.01$, N.S., not significant.

Ethics Statement

All animal studies were approved by the Institutional Animal Care and Use Committees of New Jersey Medical School-Rutgers, The State University of New Jersey (Protocol Number: 11104D0914).

Results

STIM1 and Orai1 are Expressed in Human Melanoma

We first examined expression of STIM and Orai in human melanoma. Western blot analyses showed that STIM1 and Orai1 are expressed in metastatic human melanoma cell lines, while the melanocyte cell line, HEMA-LP, displayed only a low level of Orai1 expression (Fig. 1A and B). In contrast, STIM2, Orai2 and Orai3 expression was undetectable or barely detectable in the melanoma cell lines (data not shown). We also examined expression of STIM1 and Orai1 in human melanoma tissues, using a microarray. Both molecules were immunohistochemically detected (Fig. 1C). Interestingly, STIM1, but not Orai1, showed higher expression in metastatic melanoma than in primary melanoma (Fig. 1D). This finding was confirmed using a different set of antibodies. These data suggested that STIM1 expression, but not Orai1 expression, positively correlates with melanoma progression.

SOCE Occurs in Melanoma Cell Lines

Since STIM1 and Orai1 were detected in human melanoma tissues, we examined whether SOCE occurs in melanoma cell lines. SOCE is defined as enhanced Ca^{2+} import from extracellular space after depletion of Ca^{2+} stores in the ER. Experimentally, SOCE is induced by Ca^{2+} addition after Ca^{2+} depletion from the ER with thapsigargin (Fig. 2A), an inhibitor of sarcoplasmic reticulum Ca^{2+}-ATPase (SERCA). We observed SOCE in some melanoma and melanocyte cell lines examined (Fig. 2B). Metastatic (SK-Mel-2, C8161, SK-Mel-24 and UACC2577), but not primary (WM3248, WM115 (data not shown) and WM1552C (data not shown)), melanoma cell lines showed higher SOCE peak amplitudes than the melanocyte cell line (HEMA-LP). These data suggested that SOCE is enhanced in metastatic melanoma, in accordance with the idea that activation of SOCE is related to

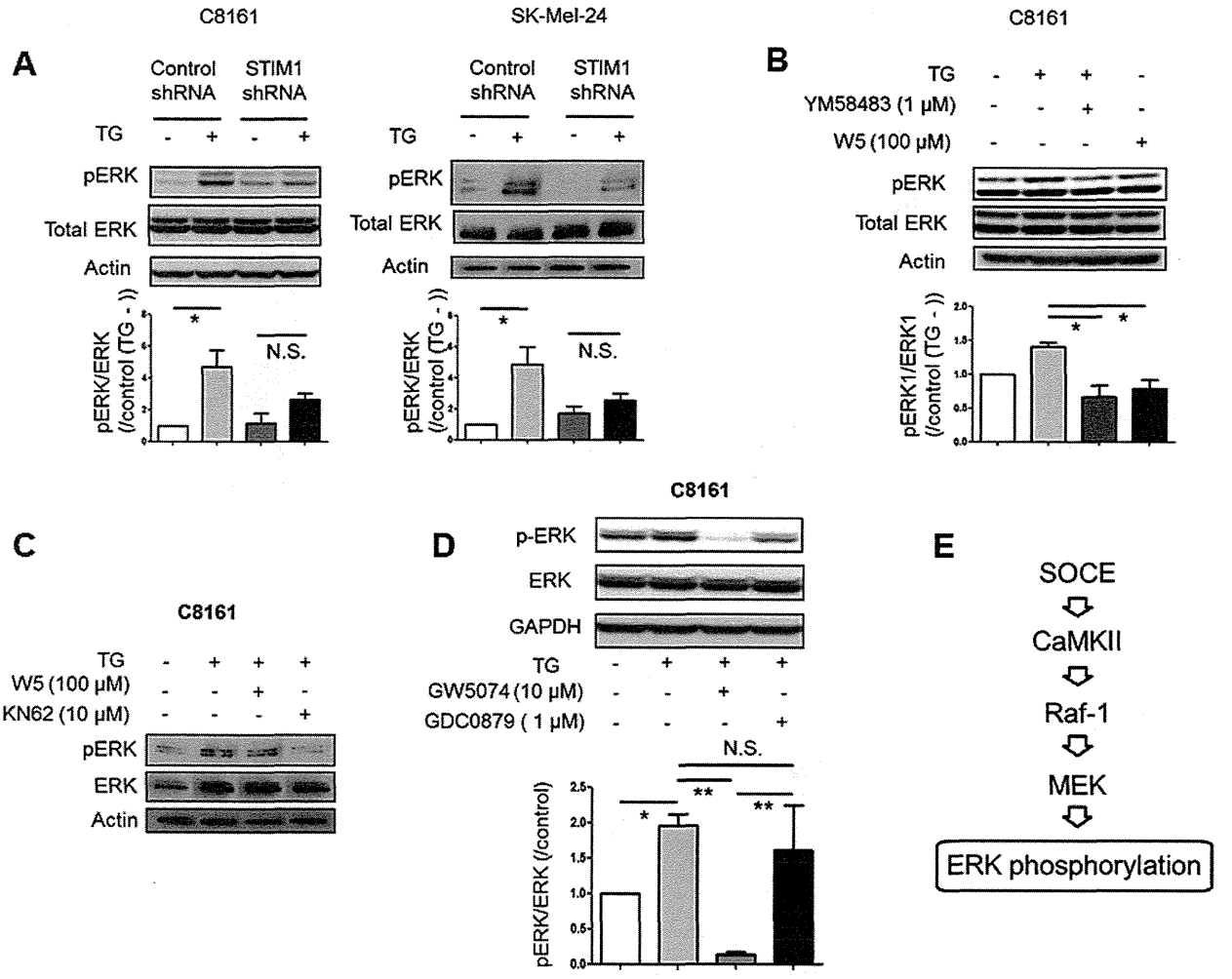

Figure 6. SOCE increases phosphorylation of ERK in melanoma. (**A**) Densitometric analyses (bar graph) of western blots show that thapsigargin increased phosphorylation of ERK1/2 in metastatic melanoma cell lines. STIM1-knockdown inhibited thapsigargin-induced phosphorylation of ERK1/2. *, $p<0.05$; N.S., not significant, n = 3. (**B**) Densitometric analyses (bar graph) of western blots show that thapsigargin-induced phosphorylation of ERK1/2 was inhibited by SOCE inhibitor YM58483 and CaM inhibitor W5 in C8161 cells. *, $p<0.05$, n = 3. (**C**) Thapsigargin-induced phosphorylation of ERK1/2 was inhibited by CaM inhibitor W5 and CaMKII inhibitor KN62 in C8161 cells. (**D**) Densitometric analyses (bar graph) of western blots show that thapsigargin-induced phosphorylation of ERK1/2 was inhibited by Raf-1 inhibitor GW5074, but not by Braf inhibitor GDC0879. *, $p<0.05$; **, $p<0.01$; N.S. not significant, n = 3. (**E**) Proposed signaling schema of SOCE-induced ERK activation.
doi:10.1371/journal.pone.0089292.g006

melanoma progression. A pyrazole compound, YM58483, which is known to inhibit SOCE in non-melanoma cells [27,28], also suppressed SOCE in metastatic melanoma cell lines (Fig. 2C and D).

STIM1- or Orai1-knockdown Inhibits SOCE in Melanoma Cell Lines

We examined whether SOCE in melanoma cell lines is regulated by STIM1 and Orai1. Ca^{2+} peak amplitude in the SOCE phase was lower in both STIM1- (Fig. 3A) and Orai1- (Fig. 3B) knockdown cells than in control metastatic melanoma cell lines (Fig. 3C). These data suggested that both STIM1 and Orai1 are involved in SOCE activation in melanoma.

Inhibition of SOCE Suppresses Melanoma Cell Proliferation

We next examined the role of SOCE in cellular functions of melanoma. We found that proliferation was reduced in STIM1-knockdown metastatic melanoma cell lines (Fig. 4A). This was not due to induction of apoptosis, because there was no significant difference of apoptosis between STIM1-knockdown and control C8161 cells after both 24 hours and 48 hours (Fig. S1). In contrast, Orai1-knockdown inhibited proliferation in C8161 cells but not in SK-Mel-2 or SK-Mel-24 cells, suggesting that STIM1, rather than Orai1, is the key determinant of melanoma proliferation. The SOCE inhibitor YM58483 (Fig. 4B) inhibited proliferation of SK-Mel-2, C8161 and SK-Mel-24 cells, further supporting the view that SOCE plays an important role in melanoma proliferation.

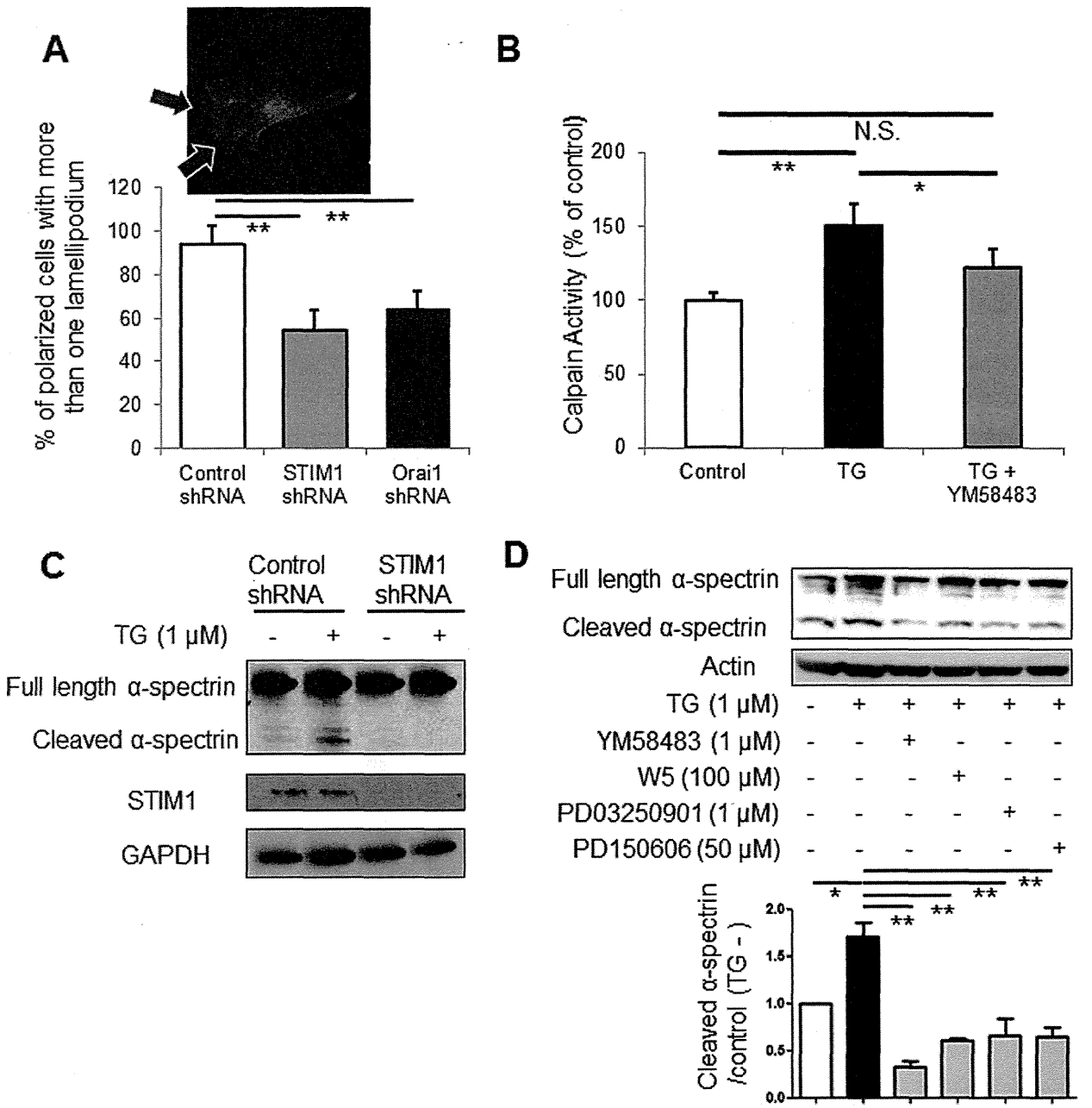

Figure 7. Proposed mechanisms of SOCE-mediated cellular functions in melanoma. (**A**) The upper panel shows actin staining of SK-Mel-2 cells. Arrows indicate lamellipodia. The lower panel shows the number of SK-Mel-2 cells with more than one lamellipodium. **, $p<0.01$, n = 331 for control shRNA, 850 for STIM1 shRNA, and 986 for Orai1 shRNA. (**B**) Calpain activity assay shows that thapsigargin increased calpain activity. Thapsigargin-induced elevation of calpain activity was inhibited by YM58483. *, $p<0.05$, **, $p<0.01$, N.S., not significant, n = 4. (**C**) Western blot analyses showed that thapsigargin (TG) increased cleavage of α-spectrin in SK-Mel-2 cells. Thapsigargin-induced cleavage of α-spectrin was inhibited by STIM1-knockdown. Representative data of 3 independent experiments are shown. (**D**) Densitometric analyses (bar graph) of western blots show that thapsigargin-induced cleavage of α-spectrin was inhibited by SOCE inhibitor YM58483, CaM inhibitor W5, MEK inhibitor PD03250901, and calpain inhibitor PD150606. *, $p<0.05$; **, $p<0.01$, n = 3.
doi:10.1371/journal.pone.0089292.g007

Inhibition of SOCE Suppresses Melanoma Cell Migration/Metastasis

Since Ca^{2+} signaling regulates migration of cancer cells [29], we also examined the role of SOCE in melanoma cell migration. We found that both STIM1- and Orai1-knockdown inhibited cell migration in metastatic melanoma cell lines (Fig. 5A and B). YM58483 also inhibited melanoma cell migration (Fig. 5C). Time-lapse video recordings showed reduced cell migration distance of both STIM1- and Orai1-knockdown cells (Fig. 5D and Videos S1, S2, and S3). We next examined whether the reduced cell migration is correlated with inhibition of metastasis. Both STIM1-

and Orai1-knockdown resulted in decreased numbers of metastatic colonies in the lungs of mice (Fig. 5E and F). These data suggested that the inhibition of SOCE suppresses melanoma cell migration and thereby reduces metastasis.

SOCE Regulates ERK Signaling in Melanoma Cell Lines

The ERK signaling pathway is known to play a major role in melanoma cells migration and proliferation [30,31]. Thus, we next examined whether SOCE affects ERK signaling. Phosphorylation of ERK1/2, which reflects activity of ERK signaling, was increased by thapsigargin in metastatic melanoma cell lines (Fig. 6A). The thapsigargin-induced ERK1/2 phosphorylation was attenuated by STIM1-knockdown (Fig. 6A) and by YM58483 (Fig. 6B), suggesting that thapsigargin-induced ERK activation occurs via a SOCE-related mechanism. Since it has been demonstrated that intracellular Ca^{2+} activates ERK signaling via calmodulin (CaM)/calmodulin-dependent protein kinase II (CaMKII) [32], we examined the involvement of these molecules in the SOCE-induced ERK activation. Thapsigargin-induced ERK1/2 phosphorylation was inhibited by W5, a CaM inhibitor (Fig. 6B and C), and by KN62, a CaMKII inhibitor (Fig. 6C), suggesting that SOCE-induced ERK activation is mediated by CaM/CaMKII. Thapsigargin-induced ERK1/2 phosphorylation was inhibited by GW5074, a specific Raf-1 inhibitor, but not by GDC0879, a specific Braf inhibitor, in C8161 cells (Fig. 6D). This is in accordance with previous findings that CaMKII can bind to and activate Raf-1 [33,34]. Similar results were also observed in SK-Mel-24 cells (data not shown), suggesting that Raf-1, rather than Braf, predominantly mediates SOCE-mediated ERK activation (Fig.6E). These data suggested that the conventional ERK signaling pathway is activated by SOCE via CaM/CaMKII.

SOCE Regulates Melanoma Cell Migration via ERK Signaling

There have been extensive studies on the mechanism of melanoma cell proliferation via ERK signaling [35,36]. However, the molecular mechanism through which ERK signaling regulates melanoma cell migration remains relatively unclear. Intracellular Ca^{2+} accelerates cell migration via calpain, a proteolytic enzyme, which promotes actin assembly/disassembly [37,38]. Therefore, it was suggested that SOCE regulates melanoma cell migration via calpain-dependent actin dynamics. This hypothesis was supported by the observation that the number of lamellipodia, which reflects the activity of actin assembly/disassembly [39,40], was decreased by STIM1- or Orai1-knockdown (Fig. 7A). In addition, we found that calpain activity was increased by thapsigargin, but was inhibited by YM58483 (Fig. 7B). Further, cleavage of α-spectrin, a target enzyme of calpain, was increased by thapsigargin, but was inhibited by STIM1-knockdown (Fig. 7C). These data suggested that SOCE regulates cell migration in a calpain-dependent manner. The question of how SOCE activates calpain then arises. Calpain was originally found as a Ca^{2+}-dependent enzyme [41], but recently it was demonstrated that ERK signaling can increase calpain activity [42–44]. We thus examined whether ERK signaling rather than intracellular Ca^{2+} itself modulates calpain activity. As shown in Fig. 7D, thapsigargin-induced α-spectrin cleavage was inhibited by YM58483, and by PD150606, a calpain inhibitor, as expected. In addition, inhibition of CaM by W5 and inhibition of MEK by PD03250901 suppressed thapsigargin-induced α-spectrin cleavage. These data suggested that calpain mediates SOCE-induced cell migration via ERK signaling, not via simple SOCE-induced elevation of intracellular Ca^{2+}.

Discussion

Our present findings show that SOCE occurs in melanoma cells and plays a pivotal role in cell proliferation and migration, most probably via ERK signaling. STIM1 and Orai1 were expressed not only in cultured melanoma cells, but also in human melanoma tissues. SOCE activity in melanoma cells was dependent on STIM1 and Orai1, and was reduced by SOCE inhibitor YM58483. Inhibition of SOCE suppressed both melanoma proliferation and cell migration. In addition, SOCE activated ERK signaling in melanoma cells, which may lead to further changes in cellular functions. Accordingly, our results suggest that melanoma progression is promoted by SOCE via ERK signaling. Recent melanoma therapies have targeted V600E-mutated Braf [1], but some patient are non-responders, and acquisition of resistance is also a problem [2]. Our data showed that SOCE occurs not only in melanoma cells bearing Braf-mutation (SK-Mel-24, UACC257, WM3248, WM115, and WM1552C), but also in non-Braf-mutation-carrying melanoma cells lines (SK-Mel-2 and C8161). In addition, we found that STIM1-knockdown inhibited ERK phosphorylation in both Braf-mutated (SK-Mel-24) and non-Braf-mutated (SK-Mel-2 and C8161) cells. These data suggested that inhibition of SOCE suppresses ERK signaling activity irrespective of the existence of Braf mutation. Therefore, targeting SOCE could potentially benefit a greater number of melanoma patients, compared to currently used Braf inhibitors.

The role of SOCE in proliferation and cell migration is well established. Abdullaev *et al.* showed that STIM1 and Orai1 regulate CRAC currents and SOCE, leading to changes in proliferation of endothelial cells [11]. In vascular smooth muscle cells, knockdown of either STIM1 or Orai1, but not of STIM2, Orai2, and Orai3, inhibited proliferation and cell migration [13]. In cancer cells, Yang *et al.* reported that STIM1-knockdown inhibited serum-induced breast tumor cell migration [16]. The same group also showed that STIM1-knockdown in hepatocarcinoma cells affects disassembly and turnover of focal adhesion [45]. Our data demonstrate that STIM1 and Orai1 have roles in proliferation and migration of various melanoma cell lines, indicating that SOCE contributes to melanoma progression. Orai1 knockdown had only a minor effect on proliferation compared to STIM1 knockdown, suggesting that TRPC channels rather than Orai1 potentially interact with STIM [46] in the regulation of proliferation. There was a discrepancy between the effective concentrations of YM58483 for inhibition of proliferation and inhibition of SOCE. This can be attributed, at least in part, to compensatory upregulation of SOCE [47], which would occur during the relatively prolonged exposure to the SOCE-inhibitory drug in MTT assay compared to the short exposure during SOCE measurement. Another concern is the fact that Orai1 deletion did not inhibit proliferation of SK-Mel-2 and SK-Mel-24 cells, whereas YM58483 treatment did. This might be explained by incomplete knockdown of Orai1.

It was recently demonstrated that, in mouse melanoma cells, SOCE occurs in lipid rafts, and ablation of the rafts suppressed tumor growth, most probably via the Akt pathway [48]. These data, taken together with ours, indicate that SOCE regulates multiple pathways in melanoma, supporting our proposal that SOCE plays a pivotal role in melanoma progression.

The upstream pathway leading to SOCE in melanoma cells remains unknown. Ca^{2+} depletion in the ER is mainly controlled by the phospholipase C (PLC)/IP_3/IP_3 receptor pathway, which is generally activated by either tyrosine kinase-type receptors or Gq-related G protein coupled receptors. Previous reports indicated that SOCE is controlled by tyrosine kinase-type receptors rather

than Gq-coupled receptors. For example, in colorectal cancer cells, epidermal growth factor (EGF) increased expression of cyclooxygenase-2 via STIM1 and Orai1 [49]. In pulmonary arterial smooth muscle cells, platelet-derived growth factor (PDGF) activated SOCE via Akt signaling [50]. In addition, both EGF [51] and PDGF [52] can increase the activity of ERK signaling in melanoma. It will be interesting to investigate the functional relationship among tyrosine kinase-type receptors, SOCE and the ERK signaling in melanoma cells.

In conclusion, our results indicate that inhibition of SOCE suppressed proliferation and cell migration/metastasis of melanoma cells, most probably via ERK signaling. We propose that SOCE is a potential target for treatment of melanoma, irrespective of whether or not Braf mutation is present.

Supporting Information

Figure S1 STIM1-knockdown did not promote apoptosis. APC Annexin V and 7-AAD staining assays demonstrated that apoptosis of STIM1-knockdown and control shRNA-transduced C8161 cells was not different. These data demonstrate that apoptosis did not contribute to the STIM1-knockdown-induced inhibition of cell proliferation. N.S. not significant, n = 4.
(TIF)

Video S1 Melanoma cell migration was inhibited by STIM1- or by Orai1-knockdown. Cellular movement was recorded by time-lapse video microscopy recording. Video S1, control shRNA, video S2, STIM1 shRNA, video S3, Orai1 shRNA.
(WMV)

Video S2 Melanoma cell migration was inhibited by STIM1- or by Orai1-knockdown. Cellular movement was recorded by time-lapse video microscopy recording. Video S1, control shRNA, video S2, STIM1 shRNA, video S3, Orai1 shRNA.
(WMV)

Video S3 Melanoma cell migration was inhibited by STIM1- or by Orai1-knockdown. Cellular movement was recorded by time-lapse video microscopy recording. Video S1, control shRNA, video S2, STIM1 shRNA, video S3, Orai1 shRNA.
(WMV)

Acknowledgments

The authors are grateful to Akane Nagasako for technical assistance in this study.

Author Contributions

Conceived and designed the experiments: MU YI KI. Performed the experiments: MU EB LX XF KO AM. Analyzed the data: MU EB SF MSD XF MI. Contributed reagents/materials/analysis tools: SF MD LX UY TF SC JG. Wrote the paper: MU EB SFD LX MI YI KI.

References

1. Chapman PB, Hauschild A, Robert C, Haanen JB, Ascierto P, et al. (2011) Improved Survival with Vemurafenib in Melanoma with BRAF V600E Mutation. New England Journal of Medicine 364: 2507–2516.
2. Nazarian R, Shi H, Wang Q, Kong X, Koya RC, et al. (2010) Melanomas acquire resistance to B-RAF(V600E) inhibition by RTK or N-RAS upregulation. Nature 468: 973–977.
3. Berridge MJ, Bootman MD, Roderick HL (2003) Calcium signalling: dynamics, homeostasis and remodelling. Nat Rev Mol Cell Biol 4: 517–529.
4. Putney JW (2005) Capacitative calcium entry: sensing the calcium stores. The Journal of Cell Biology 169: 381–382.
5. Feske S, Gwack Y, Prakriya M, Srikanth S, Puppel S-H, et al. (2006) A mutation in Orai1 causes immune deficiency by abrogating CRAC channel function. Nature 441: 179–185.
6. Prakriya M, Feske S, Gwack Y, Srikanth S, Rao A, et al. (2006) Orai1 is an essential pore subunit of the CRAC channel. Nature 443: 230–233.
7. Oh-hora M, Yamashita M, Hogan PG, Sharma S, Lamperti E, et al. (2008) Dual functions for the endoplasmic reticulum calcium sensors STIM1 and STIM2 in T cell activation and tolerance. Nat Immunol 9: 432–443.
8. Baba Y, Kurosaki T (2009) Physiological function and molecular basis of STIM1-mediated calcium entry in immune cells. Immunological Reviews 231: 174–188.
9. Di Capite J, Parekh AB (2009) CRAC channels and Ca2+ signaling in mast cells. Immunological Reviews 231: 45–58.
10. Baba Y, Hayashi K, Fujii Y, Mizushima A, Watarai H, et al. (2006) Coupling of STIM1 to store-operated Ca2+ entry through its constitutive and inducible movement in the endoplasmic reticulum. Proceedings of the National Academy of Sciences 103: 16704–16709.
11. Abdullaev IF, Bisaillon JM, Potier M, Gonzalez JC, Motiani RK, et al. (2008) Stim1 and Orai1 Mediate CRAC Currents and Store-Operated Calcium Entry Important for Endothelial Cell Proliferation. Circulation Research 103: 1289–1299.
12. Bisaillon JM, Motiani RK, Gonzalez-Cobos JC, Potier M, Halligan KE, et al. (2010) Essential role for STIM1/Orai1-mediated calcium influx in PDGF-induced smooth muscle migration. American Journal of Physiology - Cell Physiology 298: C993–C1005.
13. Potier M, Gonzalez JC, Motiani RK, Abdullaev IF, Bisaillon JM, et al. (2009) Evidence for STIM1- and Orai1-dependent store-operated calcium influx through ICRAC in vascular smooth muscle cells: role in proliferation and migration. The FASEB Journal 23: 2425–2437.
14. Suyama E, Wadhwa R, Kaur K, Miyagishi M, Kaul SC, et al. (2004) Identification of Metastasis-related Genes in a Mouse Model Using a Library of Randomized Ribozymes. Journal of Biological Chemistry 279: 38083–38086.
15. Chen Y-F, Chiu W-T, Chen Y-T, Lin P-Y, Huang H-J, et al. (2011) Calcium store sensor stromal-interaction molecule 1-dependent signaling plays an important role in cervical cancer growth, migration, and angiogenesis. Proceedings of the National Academy of Sciences 108: 15225–15230.
16. Yang S, Zhang JJ, Huang X-Y (2009) Orai1 and STIM1 Are Critical for Breast Tumor Cell Migration and Metastasis. Cancer cell 15: 124–134.
17. Fedida-Metula S, Feldman B, Koshelev V, Levin-Gromiko U, Voronov E, et al. (2012) Lipid rafts couple store-operated Ca2+ entry to constitutive activation of PKB/Akt in a Ca2+/calmodulin-, Src- and PP2A-mediated pathway and promote melanoma tumor growth. Carcinogenesis 33: 740–750.
18. Varga-Szabo D, Braun A, Kleinschnitz C, Bender M, Pleines I, et al. (2008) The calcium sensor STIM1 is an essential mediator of arterial thrombosis and ischemic brain infarction. The Journal of Experimental Medicine 205: 1583–1591.
19. McCarl C-A, Picard C, Khalil S, Kawasaki T, Röther J, et al. (2009) ORAI1 deficiency and lack of store-operated Ca2+ entry cause immunodeficiency, myopathy, and ectodermal dysplasia. Journal of Allergy and Clinical Immunology 124: 1311–1318.e1317.
20. Hoeflich KP, Herter S, Tien J, Wong L, Berry L, et al. (2009) Antitumor Efficacy of the Novel RAF Inhibitor GDC-0879 Is Predicted by BRAFV600E Mutational Status and Sustained Extracellular Signal-Regulated Kinase/Mitogen-Activated Protein Kinase Pathway Suppression. Cancer Research 69: 3042–3051.
21. Iwatsubo K, Minamisawa S, Tsunematsu T, Nakagome M, Toya Y, et al. (2004) Direct Inhibition of Type 5 Adenylyl Cyclase Prevents Myocardial Apoptosis without Functional Deterioration. Journal of Biological Chemistry 279: 40938–40945.
22. Baljinnyam E, Umemura M, De Lorenzo MS, Iwatsubo M, Chen S, et al. (2011) Epac1 promotes melanoma metastasis via modification of heparan sulfate. Pigment Cell & Melanoma Research 24: 680–687.
23. Yokoyama U, Ishiwata R, Jin M-H, Kato Y, Suzuki O, et al. (2012) Inhibition of EP4 Signaling Attenuates Aortic Aneurysm Formation. PLoS ONE 7: e36724.
24. Baljinnyam E, De Lorenzo MS, Xie L-H, Iwatsubo M, Chen S, et al. (2010) Exchange Protein Directly Activated by Cyclic AMP Increases Melanoma Cell Migration by a Ca2+-Dependent Mechanism. Cancer Research 70: 5607–5617.
25. Baljinnyam E, Iwatsubo K, Kurotani R, Wang X, Ulucan C, et al. (2009) Epac increases melanoma cell migration by a heparan sulfate-related mechanism. American journal of physiology Cell physiology 297: C802–813.
26. Mattheij NJA, Gilio K, van Kruchten R, Jobe SM, Wieschhaus AJ, et al. (2013) Dual Mechanism of Integrin αIIbβ3 Closure in Procoagulant Platelets. Journal of Biological Chemistry 288: 13325–13336.
27. Ishikawa J, Ohga K, Yoshino T, Takezawa R, Ichikawa A, et al. (2003) A Pyrazole Derivative, YM-58483, Potently Inhibits Store-Operated Sustained Ca2+ Influx and IL-2 Production in T Lymphocytes. The Journal of Immunology 170: 4441–4449.
28. He L-P, Hewavitharana T, Soboloff J, Spassova MA, Gill DL (2005) A Functional Link between Store-operated and TRPC Channels Revealed by the

3,5-Bis(trifluoromethyl)pyrazole Derivative, BTP2. Journal of Biological Chemistry 280: 10997–11006.
29. Hordijk PL (2006) Endothelial signalling events during leukocyte transmigration. FEBS Journal 273: 4408–4415.
30. Zhang W, Liu HT (2002) MAPK signal pathways in the regulation of cell proliferation in mammalian cells. Cell Res 12: 9–18.
31. McCubrey JA, Steelman LS, Chappell WH, Abrams SL, Wong EWT, et al. (2007) Roles of the Raf/MEK/ERK pathway in cell growth, malignant transformation and drug resistance. Biochimica et Biophysica Acta (BBA) - Molecular Cell Research 1773: 1263–1284.
32. Agell N, Bachs O, Rocamora N, Villalonga P (2002) Modulation of the Ras/Raf/MEK/ERK pathway by Ca2+, and Calmodulin. Cellular Signalling 14: 649–654.
33. Illario M, Cavallo AL, Bayer KU, Di Matola T, Fenzi G, et al. (2003) Calcium/Calmodulin-dependent Protein Kinase II Binds to Raf-1 and Modulates Integrin-stimulated ERK Activation. Journal of Biological Chemistry 278: 45101–45108.
34. Salzano M, Rusciano MR, Russo E, Bifulco M, Postiglione L, et al. (2012) Calcium/calmodulin-dependent protein kinase II (CaMKII) phosphorylates Raf-1 at serine 338 and mediates Ras-stimulated Raf-1 activation. Cell Cycle 11: 2100–2106.
35. Sullivan RJ, Atkins MB (2010) Molecular targeted therapy for patients with melanoma: the promise of MAPK pathway inhibition and beyond. Expert Opinion on Investigational Drugs 19: 1205–1216.
36. Meier F, Schittek B, Busch S, Garbe C, Smalley K, et al. (2005) The RAS/RAF/MEK/ERK and PI3K/AKT signaling pathways present molecular targets for the effective treatment of advanced melanoma. Frontiers in bioscience : a journal and virtual library 10: 2986–3001.
37. Potter DA, Srirangam A, Fiacco KA, Brocks D, Hawes J, et al. (2003) Calpain regulates enterocyte brush border actin assembly and pathogenic Escherichia coli-mediated effacement. J Biol Chem 278: 30403–30412.
38. Huang C, Rajfur Z, Yousefi N, Chen Z, Jacobson K, et al. (2009) Talin phosphorylation by Cdk5 regulates Smurf1-mediated talin head ubiquitylation and cell migration. Nat Cell Biol 11: 624–630.
39. Ohashi K, Fujiwara S, Watanabe T, Kondo H, Kiuchi T, et al. (2011) LIM kinase has a dual role in regulating lamellipodium extension by decelerating the rate of actin retrograde flow and the rate of actin polymerization. J Biol Chem 286: 36340–36351.
40. Batchelder EL, Hollopeter G, Campillo C, Mezanges X, Jorgensen EM, et al. (2011) Membrane tension regulates motility by controlling lamellipodium organization. Proc Natl Acad Sci U S A 108: 11429–11434.
41. Dayton WR, Goll DE, Zeece MG, Robson RM, Reville WJ (1976) A Ca2+-activated protease possibly involved in myofibrillar protein turnover. Purification from porcine muscle. Biochemistry 15: 2150–2158.
42. Chen H, Libertini SJ, Wang Y, Kung HJ, Ghosh P, et al. (2010) ERK regulates calpain 2-induced androgen receptor proteolysis in CWR22 relapsed prostate tumor cell lines. J Biol Chem 285: 2368–2374.
43. Glading A, Uberall F, Keyse SM, Lauffenburger DA, Wells A (2001) Membrane proximal ERK signaling is required for M-calpain activation downstream of epidermal growth factor receptor signaling. J Biol Chem 276: 23341–23348.
44. Glading A, Chang P, Lauffenburger DA, Wells A (2000) Epidermal growth factor receptor activation of calpain is required for fibroblast motility and occurs via an ERK/MAP kinase signaling pathway. J Biol Chem 275: 2390–2398.
45. Yang N, Tang Y, Wang F, Zhang H, Xu D, et al. (2013) Blockade of store-operated Ca2+ entry inhibits hepatocarcinoma cell migration and invasion by regulating focal adhesion turnover. Cancer Letters.
46. Yuan JP, Kim MS, Zeng W, Shin DM, Huang G, et al. (2009) TRPC channels as STIM1-regulated SOCs. Channels 3: 221–225.
47. Darbellay B, Arnaudeau S, König S, Jousset H, Bader C, et al. (2009) STIM1- and Orai1-dependent Store-operated Calcium Entry Regulates Human Myoblast Differentiation. Journal of Biological Chemistry 284: 5370–5380.
48. Fedida-Metula S, Feldman B, Koshelev V, Levin-Gromiko U, Voronov E, et al. (2012) Lipid rafts couple store-operated Ca2+ entry to constitutive activation of PKB/Akt in a Ca2+/calmodulin-, Src- and PP2A-mediated pathway and promote melanoma tumor growth. Carcinogenesis 33: 740–750.
49. Wang J-Y, Chen B-K, Wang Y-S, Tsai Y-T, Chen W-C, et al. (2012) Involvement of store-operated calcium signaling in EGF-mediated COX-2 gene activation in cancer cells. Cellular Signalling 24: 162–169.
50. Ogawa A, Firth AL, Smith KA, Maliakal MV, Yuan JX-J (2012) PDGF enhances store-operated Ca2+ entry by upregulating STIM1/Orai1 via activation of Akt/mTOR in human pulmonary arterial smooth muscle cells. American Journal of Physiology - Cell Physiology 302: C405–C411.
51. Ivanov VN, Hei TK (2004) Combined treatment with EGFR inhibitors and arsenite upregulated apoptosis in human EGFR-positive melanomas: a role of suppression of the PI3K-AKT pathway. Oncogene 24: 616–626.
52. Pirraco A, Coelho P, Rocha A, Costa R, Vasques L, et al. (2010) Imatinib targets PDGF signaling in melanoma and host smooth muscle neighboring cells. Journal of Cellular Biochemistry 111: 433–441.

PLOS ONE

Protection of Cardiomyocytes from the Hypoxia-Mediated Injury by a Peptide Targeting the Activator of G-Protein Signaling 8

Motohiko Sato[1]*, Masahiro Hiraoka[2], Hiroko Suzuki[1], Miho Sakima[1], Abdullah Al Mamun[1], Yukiko Yamane[2], Takayuki Fujita[2], Utako Yokoyama[2], Satoshi Okumura[3], Yoshihiro Ishikawa[2]

1 Department of Physiology, Aichi Medical University, Nagakute, Aichi, Japan, **2** Cardiovascular Research Institute, Yokohama City University School of Medicine, Fukuura, Yokohama, Japan, **3** Department of Physiology, Tsurumi University School of Dental Medicine, Yokohama, Japan

Abstract

Signaling via heterotrimeric G-protein is involved in the development of human diseases including ischemia-reperfusion injury of the heart. We previously identified an ischemia-inducible G-protein activator, activator of G-protein signaling 8 (AGS8), which regulates Gβγ signaling and plays a key role in the hypoxia-induced apoptosis of cardiomyocytes. Here, we attempted to intervene in the AGS8-Gβγ signaling process and protect cardiomyocytes from hypoxia-induced apoptosis with a peptide that disrupted the AGS8-Gβγ interaction. Synthesized AGS8-peptides, with amino acid sequences based on those of the Gβγ-binding domain of AGS8, successfully inhibited the association of AGS8 with Gβγ. The AGS8-peptide effectively blocked hypoxia-induced apoptosis of cardiomyocytes, as determined by DNA end-labeling and an increase in cleaved caspase-3. AGS8-peptide also inhibited the change in localization/permeability of channel protein connexin 43, which was mediated by AGS8-Gβγ under hypoxia. Small compounds that inhibit a wide range of Gβγ signals caused deleterious effects in cardiomyocytes. In contrast, AGS8-peptide did not cause cell damage under normoxia, suggesting an advantage inherent in targeted disruption of the AGS8-Gβγ signaling pathway. These data indicate a pivotal role for the interaction of AGS8 with Gβγ in hypoxia-induced apoptosis of cardiomyocytes, and suggest that targeted disruption of the AGS8-Gβγ signal provides a novel approach for protecting the myocardium against ischemic injury.

Citation: Sato M, Hiraoka M, Suzuki H, Sakima M, Mamun AA, et al. (2014) Protection of Cardiomyocytes from the Hypoxia-Mediated Injury by a Peptide Targeting the Activator of G-Protein Signaling 8. PLoS ONE 9(3): e91980. doi:10.1371/journal.pone.0091980

Editor: Xin-Liang Ma, Thomas Jefferson University, United States of America

Received December 10, 2013; **Accepted** February 16, 2014; **Published** March 14, 2014

Copyright: © 2014 Sato et al. This is an open-access article distributed under the terms of the Creative Commons Attribution License, which permits unrestricted use, distribution, and reproduction in any medium, provided the original author and source are credited.

Funding: This work is supported by Grant-in-Aid for Scientific Research on Innovative Areas of Japan (MS), Grant-in-Aid for Scientific Research of Japan (MS), the Toyoaki Scholarship Foundation (MS), The Naito Foundation (MS) and Strategic Research Foundation Grant-aided Project for Private Universities from the Ministry of Education, Culture, Sports, Science, and Technology, Japan (MEXT), 2011–2015 (S1101027). The funders had no role in study design, data collection and analysis, decision to publish, or preparation of the manuscript.

Competing Interests: The authors have declared that no competing interests exist.

* E-mail: motosato@aichi-med-u.ac.jp

Introduction

Signaling mediated by heterotrimeric G-protein plays important roles in signal integration in cells. Heterotrimeric G-proteins are activated by G-protein–coupled receptors (GPCRs) at the cell surface in response to extra stimuli. The activation of G-protein signaling is associated with nucleotide exchange on the Gα subunits leading to a conformational change in Gαβγ and subsequent transduction of signals to various effector molecules [1]. However, a novel class of regulatory proteins that directly activate heterotrimeric G protein without receptor activation has been identified [2–4]. Such molecules are expected to provide alternative signaling via heterotrimeric G-protein and regulate signal adaptation during pathophysiologic stress [5].

The importance of accessory proteins for heterotrimeric G-protein has been reported in human diseases and animal models [5]. For example, activator of G-protein signaling 1 (AGS1) is a direct activator of the Gα subunit and involved in the secretion of atrial natriuretic factor in heart failure [6,7]. Further, regulators of G-protein signaling (RGSs), the group of proteins that inhibit G-protein signaling by accelerating the GTPase activity of the Gα subunit, are involved in various cardiovascular diseases, such as hypertension, cardiac hypertrophy, and hypoxia-mediated injury [8–10].

We have been focusing on identification of accessory proteins of heterotrimeric G-proteins induced in cardiovascular diseases and have found novel activators of G-protein signaling from the hypertrophied heart and during repetitive transient ischemia [11,12]. Thus, we identified TFE3 (AGS11), an AGS protein that selectively forms a complex with the Gα16 subunit and is upregulated in the hypertrophied hearts of mice [11]. TFE3 translocates Gα16 to the nucleus, which leads to the induction of claudin-14, a component of the membrane in cardiomyocytes. This suggests that the novel form of transcriptional regulation counteracts pressure overload.

Activator of G-protein signaling 8 (AGS8) is a Gβγ signal regulator isolated from a cDNA library of rat hearts subjected to repetitive transient ischemia [12]. In response to hypoxia, AGS8 is up-regulated in the myocardium and cultured adult cardiomyocytes. AGS8 interacts directly with Gβγ and promotes Gβγ signaling in cells [12]. Suppression of AGS8 inhibits hypoxia-induced apoptosis of cardiomyocytes, suggesting AGS8 is required for hypoxia-mediated cell death [13]. AGS8 complexes with

connexin 43 (CX43) to form a transmembrane channel for multiple small molecules, including calcium, adenosine, ATP, and reactive oxygen species [14–16]. AGS8 regulates phosphorylation of CX43 in a Gβγ-dependent manner and influences hypoxia-mediated internalization of cell-surface CX43 [13]. Therefore, the AGS8-Gβγ complex plays a critical role under hypoxic conditions, making the cellular environment more sensitive to hypoxic stress by influencing the permeability of molecules passing through CX43.

Ischemic injury of the heart is associated with activation of multiple signal cascades initiating intracellular ionic and chemical changes that lead to the death of cardiomyocytes [17,18]. A previous study indicated that AGS8-Gβγ is involved in the programs leading to cell death, and the formation of the AGS8-Gβγ complex appears to be a critical step triggering the apoptotic process [13]. If a tool to manipulate the AGS8-Gβγ interaction in cells were available, it might be a promising approach for protection of cardiomyocytes against hypoxia-mediated injury.

Here, we report the identification of the Gβγ-interface of AGS8 and a peptide (AGS8-peptide) designed to correspond to the domain of interaction between Gβγ and AGS8 that protects cardiomyocytes against hypoxia-induced apoptosis. The observations indicate the importance of the AGS8-Gβγ complex in hypoxia-mediated apoptosis of cardiomyocytes as well as the potential value of targeted disruption of the AGS8-Gβγ signal for protecting the myocardium against ischemic injury.

Experimental Procedures

Materials

Anti Gβ antibody was obtained from Santa Cruz Biotechnology. Anti CX43 antibody and IGEPAL CA-630 was obtained from Sigma. Gallein was purchased from Calbiochem. Cleaved caspase-3 andtibody was obtained from Cell Signaling Technology. Recombinant $G\beta_1\gamma_2$ was obtained from Calbiochem-Merck Millipore. MTT (3-(4,5-methylthiazol-2-yl)-2,5-diphenyltetrazolium bromide) was purchased from Dojindo Molecular Laboratories (Kumamoto, Japan).

Synthesis of Peptide

The peptides were synthesized and purified by Invitrogen and peptide identity was verified by matrix-assisted laser desorption ionization mass spectrometry. The peptides were dissolved in aliquots (10 mM) and immediately frozen at −70°C.

Generation of GST-fusion Protein, Protein Interaction Assays, and Immunoblotting

The segments of AGS8 (DQ256268) were amplified by PCR and fused in frame to GST in the pGEX-6T vector (Amersham Biotech). Each GST-partial-AGS8 fusion proteins were expressed in bacteria (*Escherichia coli* BL21, Amersham Biotech) and purified on a glutathione affinity matrix. The GST fusion protein was eluted from the resin, and glutathione was removed by desalting to allow a solution-phase interaction assay [19]. Protein interaction assays and immunoblotting were performed as described previously [19,20].

Preparation of Cardiomyocytes and Delivery of Peptide to Cells

Cardiomyocytes were prepared from the hearts of 1-3-day-old Wistar rats as described previously [13]. The neonates were deeply anesthetized with pentobarbital sodium (100 mg/kg) and decapitated for cardiac tissue harvesting. The ventricular cardiomyocytes were then enzymentically dissociated and seeded at 1.0×10^5 cell in 24 mm or 4.0×10^5 cell in 35 mm plates. Prepared cardiomyocytes were cultured in DMEM/F12 including Insulin–Transferrin–Selenite (ITS), 100 units/ml penicillin, 100 mg/ml streptomycin, and 10 mM glutamine, in 5% CO_2 at 37°C. In some experiments, cardiomyocytes were incubated in a hypoxic incubator (MODEL9200, Wakenyaku, Kyoto, Japan) equilibrated to 1% O_2, 5% CO_2, and 94% N_2 at 37°C. The cells were subjected to two different hypoxic challenges. In the first protocol, cardiomyocytes were exposed 3 times to 30 min of hypoxia with intermittent 30-min periods of normoxia to capture the early events caused by hypoxia in the living cells before they died. Particularly, internalization of cell-surface connexin 43 and changes in the permeability of connexin were analyzed. In the second protocol, cardiomyocytes were exposed to 1% O_2 for 6 h followed by 12 h of normoxia to induce hypoxia-mediated apoptosis. At the end of the second protocol, apoptotic cell death was analyzed. In some experiments, approximately 24 h after preparation, peptides were delivered to cardiomyocytes by using PLUSin (Polyplus, NY, USA) according to the manufacturer's instructions. Briefly, ~1.0 μg peptide was incubated with 2.0 μl of PLUSin in 100 μl supplied buffer for 15 min and then added the mixture to each dishes. This preparation typically provided 0.5 to 1 μM of peptide in the culture medium. The amount of peptide and the incubation time for peptide-delivery were optimized by analyzing incorporation of fluorescein isothiocyanate (FITC)-conjugated peptide into cardiomyocytes. In the condition used in this study, the chemical reagent for peptide delivery did not influence the number of living cells analyzed by trypan blue stain within 4 h treatment (0.75 μM peptide; 102.0±6.7%, 1.5 μM peptide; 90.5±5.0% versus no treatment control, not statistically significant, n = 4) [21].

Immunocytochemistry

Immunostaing of cultured cardiomyocytes was performed as described previously [13]. Briefly, cells were seeded on 24×24 mm polylysine-coated coverslips. Cells were fixed with 4% paraformaldehyde for 15 min and then incubated with 0.2% Triton X-100 for 5 min. After 1 h incubation of 5% normal donkey serum, cells were incubated with primary antibodies for 18 h at 4°C. Following 1 h incubation of secondary antibody (goat anti-mouse AlexaFluor 488 or goat anti-rabbit AlexaFluor 594, highly cross-absorbed, Molecular Probes), cells were incubated with 1 μg/ml 4′,6′-diamidino-2-phenylindole, dihydrochloride (DAPI) (Molecular Probes) in PBS for 5 min. Slides were then mounted with glass coverslips with ProLong Gold antifade reagent (Invitrogen). Images were analyzed by deconvolution microscopy (TE2000-E, Nikon, Tokyo, Japan). Obtained images were deconvoluted using NIS-Elements 3.0 software (Nikon) with a "no neighbors" deconvolution algorithm. All images were obtained from approximately the middle plane of the cells.

Dye Uptake Study

Up take of CX43 permeable fluorescence dye Lucifer Yellow (LY) (Molecular Probes) was performed as described previously [13]. Briefly, cardiomyocytes were incubated with 1 mM Lucifer Yellow (LY) (Molecular Probes) for 30 min. The fluorescence of LY was determined by fluorescence microscopy (B-3A filter, TE2000-E, NIKON, Tokyo, Japan) following removal of incorporated LY and rinse with PBS. The signal intensity was quantified in 10 randomly selected fields (10×20) using NIS-Elements 3.0 software (NIKON, Tokyo, Japan). The non-specific binding of LY was determined in the presence of a connexin hemichannel blocker, 50 mM of Lanthanum (Sigma-Aldrich).

In situ Assay for Apoptosis Detection

In situ labeling of fragmented DNA in cardiac myocytes was detected by TACS2 TdT-Blue Label In Situ Apoptosis Detection Kit (Travigen, Inc., Gaitherburg, MD), that detects DNA breaks in genomic DNA by enzymatic incorporation of biotinylated nucleotides followed by the binding of streptavidin-peroxidase conjugates, according to the manufacture's instructions. Briefly, myocytes were fixed with 3.7% formaldehyde in phosphate buffered saline (PBS) for 10 min and with 70% ethanol for 5 min and then incubated in proteinase K (0.02 mg/ml) at room temperature for 5 min. The cells were incubated with 2% hydrogen peroxide for 5 min and washed with labeling buffer consisting of 50 mM Tris (pH 7.5), 5 mM $MgCl_2$, 60 mM 2-mercaptoethanesulfonic acid, and 0.05% BSA, followed by 60 min of incubation at 37°C in labeling buffer containing 150 mM dATP, 150 mM dGTP, 150 mM dTTP, 5 mM biotinylated dCTP, and 40 U/ml of the Klenow fragment of DNA polymerase I. Untreated myocytes incubated with or without 2 mg/ml DNAse in the labeling buffer were used as positive or negative controls, respectively. The incorporated biotinylated dCTP was then detected with strepavidin-peroxidase conjugate and revealed in 0.5 mg/ml diaminobenzidine for 10 min. Nuclear brown staining was viewed under a light microscope.

MTT Assay

Cardiomyocytes in 24-well culture plates were incubated in PBS (pH 7.4) containing 0.5 mg/ml MTT at 37°C. After for 2 h incubation, the PBS was removed and 100 µl of dimethyl sulfoxide (DMSO) was added to each well to solubilize dark blue formazan products. Absorbance of the colored solution was determined at 595 nm [22].

Miscellaneous Procedures and Statistical Analysis

Immunoblotting and data analysis were performed as described previously [12,13]. The luminescence images captured with an image analyzer (LAS-3000, Fujifilm, Tokyo, Japan) were quantified using Image Gauge 3.4 (Fujifilm). Data are expressed as mean ± S.E.M. from independent experiments as described in the figure legends. Statistical analyses were performed using the unpaired *t* test, F-test, one-way ANOVA followed by Tukey's multiple comparison post-hoc test. All statistical analyses were performed with Prism 4 (GraphPad Software, USA).

Ethics Statement

Animal study was approved by the Institutional Animal Care and Use Committees of Yokohama City University.

Results

The C-terminal Region of AGS8 was Required to Activate Gβγ Signaling in Cells

To determine the region of interaction between Gβγ and AGS8, we divided the rat AGS8 (DQ256268) sequence into 6 segments and synthesized the segments as glutathione *S*-transferase (GST)-fusion proteins (Fig. 1*A*). Each of GST-AGS8 peptides was subjected to a pull-down assay to examine its interaction with purified Gβγ (Fig. 1*B*). The C-terminus of AGS8 (AGS8-C) successfully pulled down Gβγ, as documented in the previous manuscript [12]. Another segment, AGS8-254, also pulled down Gβγ to a lesser extent than AGS8-C, suggesting that a potential second Gβγ-interacting domain existed in this region. However, the remaining segments failed to pull down Gβγ.

Next, the bioactivity of each of the AGS8 regions was investigated by evaluating the activation the G-protein signaling pathway in Saccharomyces *cerevisiae* [12,23]. This yeast strain lacked the pheromone receptor, but expressed mammalian Gαs in place of the yeast Gα subunit and provided a read-out of growth upon activation of the G-protein–regulated pheromone signaling pathway [23]. The peptide corresponding to each AGS8 domain was subcloned in a galactose-inducible vector and introduced into the yeast strain [24]. The bioactivity in the G-protein pathway was examined be evaluating the galactose-dependent growth of the transformed yeast. Although each segment of AGS8 was expressed in the yeast cells, AGS8-C was the only segment able to activate G-protein signaling (Fig. 1*C*). Thus, we focused on AGS-C and explored the Gβγ-interaction site in this domain.

The FN3 Domain was Important for the Interaction of AGS8 with Gβγ

The sequence of AGS8-C (A^{1359} to W^{1730} of rat ABB82299) was further divided into smaller fragments that were synthesized as GST-fusion proteins in bacteria. Two fusion proteins of GST-AGS8-C, namely, AGS8-C1 (A^{1359}– H^{1493}) and AGS8-C2 (A^{1494} – T^{1585}), were successfully synthesized and migrated as expected on SDS-PAGE. While AGS8-C1 did not pull down purified Gβγ, AGS8-C2, which represented the FN3 domain, did pull down Gβγ, indicating the importance of the FN3 domain for the interaction of AGS8 with Gβγ (Fig. 1*D*).

AGS8-peptides Blocked the Interaction of AGS8C with Gβγ

To further determine the region of interaction between AGS8 and Gβγ, we prepared multiple 29- to 30-amino–acid peptides, the sequences of which were based on the amino acids from A^{1494} to W^{1730} of the rat AGS8 (ABB82299) (Fig. 2*A*). In a screen of 11 peptides by the GST-pull–down assay, which covered the entire region from A^{1494} to W^{1730} of the rat AGS8, we found two peptides, CP1 (A^{1494}PRNITVVAMEGCHSFVIVDWN-KAIPGDV^{1522}) and CP9 (S^{1508}FVIVDWNKAIPGDVVTGYL-VYSASYEDFI^{1537}) that effectively blocked the interaction of AGS8 with Gβγ in a dose-dependent manner (Fig. 2*B*). Quantitative analysis of immunoblots confirmed the dependence of the interaction of AGS8 with Gβγ on dose (Fig. 2*C*) and indicated that both peptides had similar IC50s (CP1:6.73×10^{-6} M; CP9:2.77×10^{-6} M). We first focused on CP9 and used this peptide as the AGS8-peptide in the following experiments.

The Gβγ-interaction Site of AGS8 was Localized at the FN3 Domain of the C-terminus of AGS8

The present data suggested that the first 45 amino acids of the FN3 domain represented by CP1 and CP2 were critical for AGS8 to interact with Gβγ and mediate signal to downstream molecules. The importance of this region for AGS8-mediated signaling was further examined in the yeast cells in which growth was linked to G-protein activation [23]. A deletion mutant of AGS8-C, which lacked the first 45 amino acids of this domain, failed to activate G-protein signaling, indicating the importance of this region for mediating AGS8-Gβγ signaling in the cell (Fig. 3).

The AGS8-peptide Inhibited Hypoxia-induced Internalization of Connexin 43 in Cardiomyocytes

In a previous study, we demonstrated that AGS8 was required for hypoxia-induced apoptosis of cardiomyocytes, which was associated with changes in the permeability of CX43 [13]. AGS8-Gβγ accelerates the internalization and degradation of channel